Graduate School ETD Form 9
(Revised 12/07)

PURDUE UNIVERSITY
GRADUATE SCHOOL
Thesis/Dissertation Acceptance

This is to certify that the thesis/dissertation prepared

By ___Shanta Lewis_____

Entitled
EFFECTS OF CARBON NANOTUBES ON BARRIER EPITHELIAL CELLS VIA
EFFECTS ON LIPID BILAYERS

For the degree of ____Master of Science_____

Is approved by the final examining committee:

___Dr. Bonnie Blazer-Yost_____   _____
                 Chair
___Dr. Horia I Petrache_____   _____

___Dr. Frank Witzmann_____   _____

_____   _____

To the best of my knowledge and as understood by the student in the *Research Integrity and Copyright Disclaimer (Graduate School Form 20)*, this thesis/dissertation adheres to the provisions of Purdue University's "Policy on Integrity in Research" and the use of copyrighted material.

Approved by Major Professor(s): ___Dr. Bonnie Blazer- Yost_____

                                _____

Approved by: ___Simon Atkinson_____   05/06/2013
                   Head of the Graduate Program   Date

EFFECTS OF CARBON NANOTUBES ON BARRIER EPITHELIAL CELLS VIA

EFFECTS ON LIPID BILAYERS

A Thesis

Submitted to the Faculty

of

Purdue University

by

Shanta Lewis

In Partial Fulfillment of the

Requirements for the Degree

of

Master of Science

December 2013

Purdue University

Indianapolis, Indiana

I would like to dedicate this work to my sister Nita Lewis and my husband Dede

Frederick for their enthusiastic support and encouragement.

ACKNOWLEDGEMENTS

TABLE OF CONTENTS

LIST OF TABLES

LIST OF FIGURES

ABSTRACT

Lewis, Shanta. M.S., Purdue University, December 2013. Effects of Carbon Nanotubes in Barrier Epithelial Cells via Effects on Lipid Bilayers. Major Professor: Bonnie Blazer-Yost

Carbon nanotubes (CNTs) are one of the most common nanoparticles (NP) found in workplace air. Therefore, there is a strong chance that these NP will enter the human body. They have similar physical properties to asbestos, a known toxic material, yet there is limited evidence showing that CNTs may be hazardous to human barrier epithelia.

In previous studies done in our laboratory, the effects of CNTs on the barrier function in the human airway epithelial cell line (Calu-3) were measured. Measurements were done using electrophysiology, a technique which measures both transepithelial electrical resistance (TEER), a measure of monolayer integrity, and short circuit current (SCC) which is a measure of vectorial ion transport across the cell monolayer.

The research findings showed that select physiologically relevant concentrations of long single-wall (SW) and multi-wall (MW) CNTs significantly decreased the stimulated SCC of the Calu-3 cells compared to untreated cultures. Calu-3 cells showed decreases in TEER when incubated for 48 hours (h) with concentrations of MWCNT ranging from $4\mu g/cm^2$ to $0.4ng/cm^2$ and SWCNT ranging from $4\mu g/cm^2$ to $0.04ng/cm^2$. The impaired cellular function, despite sustained cell viability, led us to investigate the mechanism by which the CNTs were affecting the cell membrane.

We investigated the interaction of short MWCNTs with model lipid membranes using an ion channel amplifier, Planar Bilayer Workstation. Membranes were synthesized using neutral diphytanoylphosphatidylcholine (DPhPC) and negatively charged diphytanoylphosphatidylserine (DPhPS) lipids. Gramicidin A (GA), an ion channel reporter protein, was used to measure changes in ion channel conductance due to CNT exposures. Synthetic membranes exposed to CNTs allowed bursts of currents to cross the membrane when they were added to the membrane buffer system. When added to the membrane in the presence of GA, they distorted channel formation and reduced membrane stability.

CHAPTER 1. INTRODUCTION

1.1   What is Nanotechnology?

International organizations clearly define nanomaterials (NM) as those fitting the

range of 1-100 nm in any outer or inner dimension (Krug & Wick, 2011). These include

nanoobjects and nanostructured materials which have inner surface structures on the nano

scale. Nano objects categorized into nanoparticles (NPs), nanofibers, and nanoplates;

these include 3, 2 or 1 outer dimension on the nanoscale respectively (Krug & Wick,

2011).

Nanomaterials can be formed from an array of elements spanning the periodic

table, along with biological materials. The diversity of NPs increases when they are

functionalized since this gives a pure NP many more physical and chemical properties.

Once they enter a biological environment, their composition changes because of the

conjugates they form with biological material. Li and Perrett (2009) showed that when

lysozyme and β-lactogobulin adsorbed onto silica NPs they showed rapid conformational

changes at both the secondary and tertiary levels. These data indicate that NP-protein

complexes will exhibit separate functions from their individual parts.

The diversity of NMs assists in the success of nanotechnology. NMs and nanoobjects have been used in scientific research disciplines, medicine, pharmacology, engineering, textile, cosmetics, and the food industry. In one research review, Verma andPrabhat et.al (2010) explained that quantum dots can be used as photosensitizers that bind to an antibody on the surface of the target cells. When stimulated by UV light, they release oxygen species, which will be lethal to the cell. This painless technique could serve as a chemotherapeutic treatment for cancer patients. Dalton et al. (2003) illustrated that single-wall carbon nanotubes (SWCNTs) may be synthesized from carbon monoxide and lithium dodecyl sulphate as a surfactant. The fibrous SWCNT has a tensile strength of more than twice the corresponding values for steel wire and over 20 times its toughness. Their non-corrosive properties render them ideal for building high tension wires suitable for suspending bridges over wide bodies of water. Other applications of NPs are in medical imaging and energy storage. Iron oxide works exceptionally as a contrast agent for medical imaging and titanium dioxide since it is capable of harvesting sunlight in solar cells, proves to be beneficial in energy storage (Service, 2008). While nanotechnology has many valuable applications, the potential risks involved with its exposure needs to be further analyzed in order to safeguard against future risks.

The United States federal government has invested $1.8 billion in nanotechnology through the National Nanotechnology Initiative (NNI) since the NNI's inception in 2001 (Sargent, 2011). The combined budget for the past decade far surpasses this value since other U.S. companies and state governments have made additional investments (Sargent, 2011). Jaideep (2011) compared the top global government funding as of 2010 and showed that the United States alone contributed $2.3 billion. Europe, including two of the

top contributors, Germany and France, had a combined budget of $2.7 billion. Asia had a

total budget of $1.94 billion, which included the two top contributors, Japan and China,

which had a combined budget of $1.42 billion. The rest of the world contributed

approximately $1.21 billion, including Russia which had a budget of $1.05 billion of the

world's total $8.2 billion budget.

The flourishing nanotechnology industry parallels the nanotoxicology discipline.

Nanotoxicologists seek to maintain society's confidence in this new technology by

adequately addressing potential concerns about short and long term safety. While there is

an array of NMs developed from atoms found across the periodic table, only some are

commonly used in biological and medicinal applications. Hence, the focus is on those

materials which are similar to known toxic materials and with which humans commonly

come in contact. CNTs are the most commonly found NPs in workplace air, and they are

the NPs of interest in this research study. These have a greater chance of coming into

contact with barrier epithelial tissue via inhalation or ingestion and may eventually get

into the blood stream (Krug & Wick, 2011).

1.2   Why Nanotoxicology?

Nanotoxicologists have a long way to go before there is a full understanding of

the effects of carbon nanoparticles (CNP). Service (2008) claims that with potentially

thousands of novel nanomaterials inundating the global markets, safety regulators have

not fully understood which are safe and which are potentially toxic. This uncertainty may

be detrimental to the progress of this new technology as users may magnify any threat if

the hazardous nature of the materials is not clearly understood. Since the advent of this

new technology, many researchers have investigated and attempted to elucidate the toxicity of various nanoparticles. Coccini, Manzo and Roda (2013) showed the result of exposing human A549 pneumocytes to 1, 10 or 100 µg/ml carbon nanoparticle concentrations for 24 or 48 hours (h). The study involved exposures of various doses of the test nanomaterials (pristine MWCNTs, MW-COOH, MW-NH$_2$, CB, or SiO$_2$). The *in vitro* result showed that all the CNTs (pristine and functionalized) showed mild to moderate cytotoxicity on the cell line. The *In vivo* result showed that the intratracheal instilled MWCNTs could cause lung toxicity associated with inflammation. These data indicate that caution should be taken before considering that the functionalization of nanomaterials is a safe way to improve biocompatibility.

So far researchers from around the world are undertaking the task of sorting out the toxic NPs from the less toxic ones. Toxicologist Andre Nel and his group have devised methods of testing the effect of thousands of different materials on cell lines at a single time by using a battery of assays (Service, 2008). Their results indicated that there were many nanomaterials, including CNTs, which were toxic. In one study, when the lung tissue of rats were flushed with the nanotubes, researchers found that the nanotubes clumped together, making it difficult for the animal's immune system to remove them from its body. Qu et al. (2009) also showed that, when inhaled, SWCNTs and MWCNTs caused interstitial inflammation and epithelioid granulomas. While the effect of the CNTs were dependent on the mode of entry, i.v. injected CNTs were less effective than inhaled or ingested particles. This may be attributed to the accumulation of these particles *in vivo* due to the overwhelmed clearance mechanisms.

Bhabra et al. (2009) illustrated that fibroblasts indirectly exposed to cobalt-chromium (CoCr) alloy particles through BeWo cells had significant DNA damage. The BeWo cells were grown on filters suspended in a well in which fibroblasts were grown on the bottom. Data from this experiment showed that NPs did not pass through the BeWo permeable supports; instead, the damage to the underlying fibroblasts was mediated through junctional complexes involving pannexin and connexin, gap junctions and hemichannels and purinergic signaling. These data show that NPs may have an indirect effect on intracellular components via cell signaling. The data can also be interpreted to show that NPs used in the body are sometimes too large to be removed; therefore, they remain in the blood. This advantage of organ targeting will then become a disadvantage since these particles will remain exposed to certain organs that are not the main target.

Silver nanotubes are widely used for their germicidal properties. Ingested silver metal may damage epithelia of the gastrointestinal tract. Chronic exposure to silver may also affect the liver, kidney and spleen, as well as, result in irreversible discoloration of the skin (Panyala, Peña-Méndez & Havel, 2008). Another popular application, is the use of silver NPs in food containers and clothing, for their anti-germicidal properties (Panyala, Peña-Méndez & Havel 2008). Cosmetologists are also implementing TiO_2 NPs into sunscreen products for their UV-B protection property (Popov et al., 2005).

1.3   Why carbon nanotubes?

CNTs have many non-biological applications, for instance, nanosized electronic devices. Experimental results showed that metallic SWCNTs can carry currents of up to

10^9 A/cm^2 whereas normal metals carry a max current of 10^5A/cm^2. Another non-biological use of CNTs is its ability to store hydrogen, which is capable of fueling cells that power vehicles and mobile computers (Yao, Kane & Dekker, 2000; Liang et al., 2001). Biological applications include drug delivery, which are assisted by functionalization of the CNTs. For instance, color-tagged SWCNTs for Raman-based protein detection *in vivo* and *in vitro.* (Liu, Tabakman, Welsher, & Dai, 2009).

CNTs may be one of the most widely used NPs. It has been postulated that by 2020, there will be a compiled budget of $10 billion spent on their applications (Tantra & Cumpson, 2007). Given that the supply of CNT-based products will increase, there is a concern about the prevalence of nanotubes in the air, and more specifically in factory workplace air. Based on this concern, we investigated the toxic effect of CNTs on barrier epithelia. Tantra and Cumpson (2007) assert that CNTs pose the greatest toxic threat when they come into contact with our bodies. When settled on our skin, inhaled or ingested they could accumulate on epithelial tissue. Inhalation or ingestion creates greater threats than the other modes of exposure.

The mucociliary clearance mechanism (MCM) helps to rid the lungs of particulate matter before they enter the alveoli. If the MCM is successful in its clearance, the mucus that is brought out from the lungs is generally swallowed unconsciously. Otherwise accumulated NP in the lungs tends to agglomerate and develop fibrous tissue as well as granulomas (Krug & Wick, 2011; Tantra & Cumpson, 2007). In our study we used two cell lines that mimic the *in vivo* physiology of the barrier epithelial tissue. Cell characterization was done to show hormonal as well as physical similarity to the tissue.

1.4   Electrophysiology

Hans Ussing developed the Ussing chamber initially for the measurement of vectorial ion transport through frog skin (Ussing, & Zerahn, 1951). Its current use has revolutionized our understanding of electrolyte movement in epithelia. Ussing chambers are now being employed for measurements of ion movement across epithelial monolayers. We used this method to evaluate our cell lines by the electrophysiology technique. This technique measures transepithelial electrical resistance (TEER) as well as the short circuit current (SCC) (Li, Sheppard, & Hug, 2004). TEER is a measure of the integrity of the cell monolayer and can be determined by the tight junction resistance, intercellular space resistance and resistances of the apical and basolateral membranes. SCC measures ion flux across the cells at the basal level as well as in response to hormonal and effector stimulation and inhibition (Blazer-Yost et al., 2011).

The Ussing chamber is composed of two functional halves: the electrical circuitry and the Ussing chamber itself. The electrical circuitry is used to measure the tight monolayer's TEER as well as the SCC when a voltage is applied to the cell monolayer that is clamped in the Ussing chamber. An increase in the short circuit current indicates that there is movement of negatively charged ions in the secretory direction or movement of positively charged ions in the absorptive direction.

The final SCC value is a measurement of net ion flux, potentially made up of multiple individual ion movements. Therefore, after inhibiting certain channels hypothesized to be in a particular cell line and/or stimulating ion channels with known secretagogues, these techniques then can be used to characterize the presence of channel proteins.

1.5   Carbon nanotubes' effect on the MPK cell lines

Previous nanotoxicology research done in our laboratory showed the effects of long SW and MW CNTs on the mouse principal cell type of the kidney cortical collecting duct clone 4 (mpk CCD_{cl4} or MPK) cell line. The cells were grown on Costar-corning (24 mm polycarbonate inserts with pore size of 0.4µm) permeable transwell membranes (Acton, MA), and the feeding medium was replenished every 2-3 days. Cells were allowed to grow for 14 days so that the monolayer could become confluent then, 48 h before day 14, cells were incubated with various concentrations of fullerenes, SW and MW CNTs ranging from 40µg/cm^2 (100µg/ml) to 40pg/cm^2 (0.1µg/ml). On the day of electrophysiology, the permeable supports were cut out from the transwells and mounted onto Ussing chambers. The cells were allowed to stabilize for 0.5 to 1 h before TEER and SCC were measured (Blazer-Yost et al., 2011).

The MPK cells showed a marked decrease in TEER after exposures to select NP concentrations. The 0.4 ng/cm^2, 4 ng/cm^2, and 0.04 µg/cm^2 concentrations of the SWCNTs cause a significant decrease in the resistance. The MWCNTs concentrations, 40 µg/cm^2 to 0.4 ng/cm^2 also caused a decrease in resistance. The fullerenes also decreased the MPK TEER due to exposures to the 0.4 ng/cm^2, 4 ng/cm^2 and 0.04 µg/cm^2 concentrations. There were no changes in the levels of the tested cytokines or lactate dehydrogenase (LDH) leakage, indicating that none of the NP concentrations caused any cellular damage (Blazer-Yost et al., 2011). The data showed that the decrease in TEER was not sufficient to cause cell death; rather it showed a compromised resistance in the cell barrier function.

Epithelia have the remarkable ability to switch from absorption to secretion. While both cellular actions resemble each other when the appropriate ions are moved, they indicate the net movements of ions as well as compensatory water flux. The individual ion movements may be determined by applying certain drugs that influence either the absorptive (positive ion) or secretory (negative ion) pathway (Li, Sheppard, & Hug, 2004). Antidiuretic hormone (ADH) was used as a secretory agent because it causes a multiphasic response of chloride secretion via the cystic fibrosis transmembrane regulator (CFTR) and sodium absorption via the epithelial sodium channel (ENaC).

While cell survival had not been compromised, the effects of the NPs were clearly detected at the molecular level. Proteomic analysis of the samples resulted in a collection of nearly 1,878 proteins that were compared and categorized, 254 of which were altered across all NP concentrations. The number of proteins whose expression declined was inversely proportional to NP concentration. Some proteins affected were ribosomal proteins which are important for protein synthetic processes, as well as histone family proteins that are significant in DNA stability and repair.

The proteomic results demonstrated that the NP were effective at physiological concentrations, the lowest concentrations which have ever been studied (Blazer-Yost et al., 2011). Most researchers used higher concentrations than the highest dose used in this study, $40\mu g/cm^2$ (100 µg /ml). There were high levels of agglomeration of CNTs at $40\mu g/cm^2$ and $4\mu g/cm^2$ exhibiting more of a micro effect on the cells than a nano effect.

1.6   <u>NPs' effect on the lipid bilayer</u>

NPs were added with the media to the apical side of the MPK cell monolayer and had clear effects on the cells' resistances, which indicated that they may impair junctional or membrane proteins. However, there were many intracellular proteins that were altered in response to NP exposures, including histone cluster1; H2Bf (the proteins responsible for the nucleosome structure of the chromosome); LIM homeobox 9 (a protein which has a role in gonadal development); and MYB binding protein (P160) 1a (a protein described by the UniProt (2012) as a transcription repressor via interactions with specific DNA binding proteins) (Geer et al., 2012). Every aspect of the cell is in some way connected. Hence, these data suggest that the NPs may have induced an effect from the cell's surface which might have been received within the cell.

The plasmalemma may be the key component in understanding the connection between extracellular exposure and intracellular changes. Cell membranes are predominantly comprised of lipids and proteins, and the cellular protein/lipid composition is determined by the function of the tissue. The chemical compositions of various cell membranes have different protein/lipid ratios. Myelin membranes have a high protein/lipid ratio, ~0.23, in comparison to the outer membrane of the mitochondria, ~1.1, which is very enzymatically active (Guidotti, 1972).

Lipids make up 25% to 80% by weight of cell membranes. They are usually amphipathic, composed of both hydrophobic (polar tail groups) and hydrophilic (non-polar head groups) parts thus allowing them to readily form surface monolayers when spread on water or polar solvents. When lipids are added to an aqueous environment they form micelles, which allow the hydrophilic heads to remain exposed while the tails are

tucked within the globular structures. Alternatively the lipids interact with the polar liquid to form a surface monolayer, which, when compressed, arranges to form bilayers. These bilayers have properties that closely resemble natural membranes (Hall, & Baker, 1977). Therefore, artificial lipid bilayers can be used to understand how CNTs interact with the lipid component of cell membranes.

1.7 CNTs can traverse and enter the cell

Dawson, Salvati, and Lynch (2009) showed that NPs change the membrane structures and therefore could influence effects in membrane lipid and protein functions. In their study, positively or negatively charged polystyrene NPs (~20 nm in diameter) were added to liposomes, which are spherical lipid bilayer compartments containing aqueous centers. Results showed that there was a charge-dependent reconstruction of the locally bound membrane surface. Negatively charged NPs that were added to fluid areas of the membrane caused gelation and positively charged NPs caused gelled membrane surfaces to become fluid. Data analysis showed that the membrane charge was dependent on the density of the charge. Greater charges resulted in greater degrees of phase changes.

NPs may cause changes in the cell membrane and this effect was noted in the decreased TEER in the MPK cells (Blazer-Yost et al., 2011). Dawson, Salvati, and Lynch (2009) further assert that a local phase change in the membrane may be a catalyst for many other changes in the cell. The cell membrane houses signaling proteins, receptors and ion channels. The fact that the NPs have the potential to affect the membrane lipids indicates that it has the potential to affect biological processes also. The risk involved should be carefully analyzed.

CHAPTER 2. METHODS

2.1   Carbon nanotubes preparation

The raw and pristine short MWCNTs were obtained from Dr. Somenath Mitra
(New Jersey Institute of Technology) and the long SW and MW CNTs were purchased
from SES Research (Houston, TX) and were used with no further purification. As
reported by the manufacturer, the short nanotubes were 1-5 µm and the long nanotubes
were 5-15 µm long. The diameter of the MW was 40-60 nm and that of the SW
nanotubes was less than 2 nm. 5 mg of the CNTs was added per 1 ml FBS (Fetal Bovine
Serum) which was purchased from Gemini Bioproducts, (West Sacramento, CA). The
solution was placed in a 2ml microcentrifuge tubes from Dot scientific (Burton, MI). An
equal FBS volume was sonicated for 10 pulses to coat the sonicator probe; then the CNT-
FBS mixture was sonicated for 20 pulses. The sonication was done using a Branson
Sonifier 450 with the time set to hold, duty cycle 30% and output control set to level 3.
The solution was then serially diluted with FBS at a ratio of 1:10 eight times. The probe
was washed with ethanol and wiped down with a Kim wipe after each concentration had
been made. The new solutions were transferred to Borex borosilicate glass culture
testubes, 12 x 75 mm, and autoclaved for 25 min. The CNT-FBS solution consisted of 2%
of the final cell culture media's FBS volume. This solution was added to a cell culture
media solution containing 3% FBS to make a final media solution with the total of 5%,

FBS. By using the following equation $\frac{5mg}{ml} * 2ml = 100ml * x$, the total concentration of

CNTs in 1 ml, x, was able to be calculated. This concentration was calculated to be 100

μg/ml. The samples were then serially diluted 10 fold, eight times. Therefore, the amount

of CNTs in 1 ml of each of the dilutions was calculated to be 100 μg/ml to 10 pg/ml.

The pristine CNTs were purified after they were first purchased from Cheap

Tubes (Brattleboro, VT). Between 5-250 mg of the CNTs were weighed out and placed in

diluted nitric acid, hydrochloric acid or sulfuric acid. A chelating agent was dissolved in

acid to make the saturated solutions. The mixture was placed in a microwave set to 50%

of 900 W and a pressure of 30 psi for 20 min. After the reaction the mixture was filtered

and the solid phase, CNTs, was analyzed for purity. The purified tubes were not

functionalized in the purification process.

2.2   Zeta potential

Zeta potential is the potential between the particle surface and the medium in which

it is dispersed. This measurement was done using a zetasizer Nano ZS90. NPs were

prepared using the method described in section 2.1. Samples included concentrations

ranging from 4μg/cm^2 (100μg/ml) down to 4pg/cm^2 (100 pg/ml). Samples were stored in

4°C refrigerator and were brought to room temperature prior to use. 1.5 ml of each

sample was taken up using a graduated 2 ml plastic pipette purchased from Fisher

Scientific (Waltham, MA) and added to a 12 mm square polystyrene cuvette. The cuvette

was placed in the zetasizer and the sizes of the CNTs were measured. Zeta potential

measurements were then done using a dip cell from the Universal dip cell kit (zen1002)

purchased from Malvern Instruments (Malvern, Worcestershire). The dip cell was

inserted into the cuvette and the zeta potential was measured.

2.3   Transmission electron microscopy

The formvar-carbon coated, 300 or 400 mesh, nickel or copper grids were

obtained from Electron Microscopy Science (Hatfield, PA). Short multi-wall CNTs were

prepared at 5mg/ml concentrations and diluted in serum free media or 2% FBS media.

The final concentrations were high- 4 μg/cm^2, medium- 4 ng/cm^2 and low- 4 pg/cm^2. The

grids were placed on the bottom of a 6-well Corning glass plate. 2 ml of the CNT samples

were placed on the grids and were incubated for 48 h. The media was then extracted

using a vacuum system, and then the grids were air dried and stored in the grid casing in

preparation for imaging. The CNTs were viewed using a Tecnai G2 12 Bio TWIN with a

FEI, Hillsboro, OR equipped with AMT CCD Camera (Advanced Microscopy

Techniques, Danvers, MA). Comparisons were made between the concentrations and

solvents of each sample.

2.4   Cell culture media preparation

The tissue culture media was made in double distilled H$_2$O by adding 1 packet

DMEM/F-12) and 1mM glutamax which were purchased from Life Technologies (Grand

Island, NY) and 2.40g/L NaHCO$_3$ purchased from Sigma Aldrich (St. Louis, MO). T84

cell culture media was composed of 5% FBS, while Calu-3 cell culture media comprised

of 15% FBS. The T84 media solution contained 0.4% and the Calu-3 cell culture media

contained 1% penicillin/streptomycin, purchased from Sigma Aldrich (St. Louis, MO).

T84 media was completed with 12 mg/L ciprofloxacin purchased from Mediatech, Inc

(Herndon, VA). The Calu-3 media was completed with 0.5 mM non-essential amino

acids and 0.5 mM sodium pyruvate purchased from Invitrogen (Carlsbad, CA). The

media was sterile filtered and stored at 4°C.

2.5   Cell culture method

Cell lines, Calu-3 and T84, were purchased from American Type Culture

Collection, ATCC (Manassas, VA). Cell culture flasks and 6-well permeable tissue

culture supports (24 mm inserts, polycarbonate, pore size- 0.4 µm) were obtained from

Costar-Corning (Acton, MA).

The cell culture media flasks were placed in a 37°C water bath for 1-2 h to allow

the media to equilibrate. The cells were carefully maintained in a sterile environment and

grown in culture flasks then transferred to permeable tissue culture supports, where they

were grown for 14 days in a humidified incubator at 37°C and 5% CO_2 until they became

confluent. Cells were fed every two to three days by replacing the apical and basolateral

media (only the basolateral media was replaced in the Calu-3 cells), as well as the media

in the flasks, using a glass pipet that was flamed every 3 seconds. Before each media

change, the cells in the flasks were monitored for cell growth and development using a

Nikon light microscope, Phase Contrast 2, ELWD, 0.3M (Japan). Cells were split after

the cells grown in flasks had become 95% confluent (7-10 days), and seeded onto 1 or 2

six-well permeable tissue culture supports plates and one flask.

To split the cells for seeding, the media was extracted and the cells were rinsed

with 10 ml of Hanks balanced salt solution (HBSS) obtained from Mediatech Inc.

(Manassas, VA) 2 ml of 10X trypsin-EDTA (0.5%) obtained from Life Technologies (Grand Island, NY) was added to 10 ml HBSS and then added to the cells. The flask was placed in the incubator for $10 - 15$ min during which time the cells were occasionally observed under the microscope. After 90% of the cells had released from the bottom of the flask, 10 ml of serum-containing cell culture media was added to the flask to stop the trypsinization. The cell suspension was placed in a Costar-Corning 50 ml centrifuge tube and the cells were spun at 1000 rpm for 5 min. The supernatant was discarded and the cell pellet was suspended again in 10 ml of fresh cell culture media. 2.5 ml of the suspended cells were seeded into a culture flask containing 12.5 ml of cell culture media. An additional 16.5 ml of cell culture media was added to the remaining cell suspension and 2 ml of cells were seeded into each Transwell. Cells were allowed to grow on filters for 14 days to form a monolayer exhibiting tight junctions between cells. They were then used for cell line characterization and CNT exposure dose response using the electrophysiology technique.

2.6   Acid treated short CNTs

The CNTs were acid treated to simulate the *in vivo* chemical conditions that they may encounter while passing through the digestive system. The raw and pristine NPs were used without further modification. 100µl of simulated gastric fluid (0.2% w/v NaCl in 0.7% (v/v) HCl, from the Ricca Chemical Company (Arlington, TX) was added for every 5mg of CNTs and the mixture placed in a covered glass vial. The vial was placed on a shaker and allowed to oscillate for 2 h at room temperature. After the incubation, 100µl simulated intestinal fluid Test Solutions (TS), United States Pharmacopeia test

solution was added to the vial and put on the shaker for an additional 1h. After 1 h, a volume of FBS was added to the vial to make a final volume of 5mg/ml of solution. This CNT solution was further prepared in a similar manner to the CNT preparation method in section, 2.1.

2.7   Electrophysiology

Electrophysiology is a technique used to measure the TEER, which is a measure of the cell integrity and barrier function. This measurement is a composite of the resistances across the cell apical and basolateral membranes, intercellular spaces as well as the tight junctions. This technique also measures SCC, which measures ion flux across the cellular monolayers in response to hormonal stimulation. After cells were seeded onto the permeable supports, they were allowed to grow for up to 14 days until they became confluent. 48 h before cells were used for electrophysiology, the CNTs dissolved in cell culture media, were added to the apical media compartment of the cells. In preparation for the electrophysiology experiment, the Ussing chamber was rinsed with warm distilled water and the water jacket system was allowed to equilibrate to 37°C. Empty Ussing chambers were attached to the DVC-1000 voltage/current clamp (World Precision Instruments) via the voltage and current electrodes on either side of the chamber. The air was turned on and 15-20mL of FBS free media was added to the reservoir. The electrodes were calibrated to ensure that the resistance measurements reflected the activity within the tissue only. The electrodes were attached to the DVC-3 and it was turned on. The system was checked for noise and offset voltages, which may have occurred by improper storage of the electrodes, by observing the display screen on the DVC-1000. The fluid

resistance compensation on the DVC-1000 was adjusted to zero to cancel the offset

voltage generated by the media and electrodes.

The media was then drained out of the chamber and the set-ups were cleared in

preparation to mount the cells. The plates were retrieved from the incubator and the

inserts with the confluent cells were cut out from the transwells then mounted onto

Ussing chambers. The voltage and current electrodes were attached to either side of the

membranes. 10 ml of serum-free media was added using 10 ml syringes to either side of

the U-shaped glass tube, ensuring that an even hydrostatic pressure was applied to the

cells at all times. The spontaneous transepithelial potential difference was clamped to

zero and the resultant short circuit current was monitored. The media bathing the cells

were maintained at 37^oC via the water-jacketed buffer chamber supplied by a heated

water bath. The media was also circulated by a gas lift composed of 95% O_2 and 5% CO_2;

this air also maintained constant pH balance in the media and supplied oxygen to the cells.

A 2 mV pulse was applied every 200 s to the cells by the DVC-1000. The resultant

deflection of the SCC was used to calculate the cells' TEER by using ohm's law: $V = IR$.

After the basal current had been stabilized, the inhibitors were added at time = -10 min

and the secretagouge was added at time = 0 min. The data of each cell monolayer

responses to the various hormones and inhibitors were analyzed and the changes in SCC

were used to determine what channels were present and functional in that cell line. In the

dose response experiment, changes in the TEER as well as the SCC were analyzed to

determine the effect of each CNT concentration on that cell monlayer.

2.8   Characterization of Calu-3 Cells

The Calu-3 cell line was originally derived from a pleural effusion associated with a 25 year old male with a lung adenocarcinoma (Shen at al., 1994). The cells were grown at an air-liquid interface, meaning, the cell culture media was only added to the basolateral compartment of the Transwell permeable support when cells were fed. Cells were fed at an air-liquid interface during their first media change after seeding. This was done by adding cell culture media only to the basolateral compartment of the Transwell. They were cultured to confluency on the permeable supports as described in section 2.5 *Cell Culture Method*. Confluent Calu-3 cells formed a polarized monolayer with tight junctions exhibiting TEERs of > 800 $\Omega.cm^2$. The following mediators were used to test for the presence of specific ion channels in the cells: Epinephrine, which was purchased from Bio/Data (Horsham, PA); Forskolin and 5-Nitro-2-(3-phenylpropylamino) benzoic Acid (NPPB) purchased from Biomol International (Pike Plymouth Meeting, PA); and CFTR inh-172, purchased from CalBiochem (Billerica, MA) tannic acid was purchased from Sigma Chemical Co. (St. Louis MO), ionomycin and bapta were purchased from Enzo Life Sciences (Farmingdale, NY); LY294 002 and U73122 were purchased from Sigma Aldrich, (St. Louis, MO). The time and quantity of each mediator added is described in chapter 3, *Results.*

2.9   Fluid secretion

The level of apical fluid secretion that resulted due to the stimulation of Calu-3 cells with epinephrine was measured. Cells were allowed to grow for 14 days to allow them to form a confluent monolayer on the Costar-Corning Transwell polycarbonate

permeable membranes. In the first fluid secretion experiment the apical fluid secretion

was first removed from the experimental wells. The cell monolayer was then

basolaterally stimulated with 10^{-6} M epinephrine, then the plate was swirled for 2 or 5

min. The total resultant apical fluid secretion was collected and weighed. In the second

fluid secretion experiment, the initial apical fluid secretion was not removed before

stimulating the monolayer. The cell monolayer was stimulated with 10^{-6} M epinephrine

and the plate was swirled for 2 or 5 min. Following, the total apical media plus the

resultant secretion was collected and weighed. The control Transwells were only swirled.

A histogram of the weight of the fluid secretion, mg, was plotted to show the results.

2.10   cAMP assay

Cyclic adenosine monophosphate (cAMP) was measured using a kit, enzyme-

linked immunosorbent assay, ELISA, Enzo Life Sciences (Farmingdale, NY). All

reagents were brought to room temperature. The lysis buffer, 0.1M HCl with 1%Triton-x-

100 and assay wash buffer were made fresh the morning before the assay was done.

Confluent Calu-3 cells grown on Corning 6-well transwell plates for 14-15 days were

used. Cells were stimulated for 20 second and 1 min intervals by adding 10^{-6} M

epinephrine to the basolateral media compartment followed by gentle swirling for the test

time. The apical fluid secretion and basolateral media were removed and stored. 1 mL

and 3 ml of HBSS were added to the apical and basolateral side, respectively, then

swirled to wash the cells. After it was removed, the washing was repeated. Following the

wash steps, 750µl of HCL-Triton-x-100 was added to the apical side of the cells and the

plate was returned to the incubator for 10 min. After cell lysis, a rubber policeman was

used to remove the lysed cells from the membrane. Five clockwise and counterclockwise scraping motions were done to remove the cells and the cell supernatant was extracted, centrifuged, and used for the cAMP assay. The standards were prepared by preparing 1:10 serial dilutions for the first test tube and then 1:4 for the remaining four test tubes. The neutralizing reagent and non-specific binding reagent was added to the specified wells followed by 100μl of standards and samples to the appropriate wells.

This was followed by adding 50μl of the blue conjugate and the yellow antibody, respectively; the plate was then sealed and incubated for 2 h on a plate shaker. After incubation, the contents of the wells were removed and the wells were washed by adding 400μl of wash buffer to every well. The washing was repeated two more times. After the final wash, 5 μl of the blue conjugate was added to the TA wells, and 200 μl of the substrate was added to each well, then the plate was incubated for 1 hour. 50V of stop solution was added to each well. The optical density of the colored product was measured at a wavelength of 450 nm using a microplate reader. The concentration of cAMP was inversely proportional to the brightness of the color of the wells. The OD values were used to calculate the concentration of nucleotide produced for 20 sec and the 1 min stimulation times and deductively the presence of the cAMP.

2.11 Characterization of T84 cells

The T84 cell line is a transplantable human carcinoma cell line derived from a lung metastasis to a colon carcinoma in a 72 year old male. Tumor tissue was inoculated subcutaneously and serially transplanted in BALB/c nude mice, and after 23 passages the cell line was created (Murakami and Masui, 1980). The cells exhibit tight junctions and

desmosomes between adjacent cells, contain receptors for many peptide hormones and neurotransmitters, and maintain vectorial electrolyte transport, (Dharmsathaphorn et al., 1984). Cells grow to confluence as monolayers in 14 days and have transepithelial electrical resistance in the range of 500-1000 $\Omega.cm^2$. T84 cells were treated with the following hormones and inhibitors in order to characterize the cell line and determine the dose dependent effect of CNTs: Secretin and Amiloride were purchased from Sigma Aldrich (St. Louis, MO), NPPB was purchased from Biomol International (Pike Plymouth Meeting, PA); Tannic acid was purchased from Sigma Chemical Co. (St. Louis MO), GLyH-101 and CFTR inh-172 were purchased from CalBiochem (Billerica, MA). The time and quantity of each mediator added is detailed in chapter 3, *Results.*

2.12 Dose response T84

48 h before electrophysiology measurements were done, 2 ml of the CNT-media solution was added to the apical compartment of the cell monolayer and the plates were carefully labeled with the CNT concentrations, NP type (raw, pristine or acid treated) date and start time of incubation. The plates were returned to the incubator and precisely two days later, the permeable supports with cell monolayers were mounted onto Ussing chambers for TEER and stimulated SCC measurements.

2.13 Cyokine assays

The Quantikine ELISA Immunoassays, interleukin-8 (IL-8) and tumor necrosis factor-alpha (TNF-α) kits were purchased from R and D Systems, (Minneapolis, MN). These were used to measure the levels of two cytokines in the apical and basolateral cell

media solutions for the confluent T84 cell cultures incubated with pristine short MWCNT

for 48 h. The concentrations of the nanotubes used were $4\mu g/cm^2$, $4ng/cm^2$, $4pg/cm^2$ and

a control, which was only cell culture media. The apical and basolateral media were

extracted and assayed by diluting it 1:1. The assays were conducted in triplicate

according to the specifications given in the protocol. All reagents, standards, wash buffer

and assay diluents were prepared using the formulas given in the manual. 50 µl of the

assay diluent was added to each well followed by 200 µl of standard sample or control to

the appropriate wells. The mixture was covered with an adhesive strip and incubated for

2 h on a shaker at room temperature. After the incubation, each well was aspirated and

washed four times with 400 µl wash buffer. After each wash, the remaining wash buffer

was removed by blotting the plate against clean paper towels. 200 µl of TNF-α conjugate

was added to each well and covered with a new adhesive strip and incubated for 1 hour.

The wash step was repeated and then 200 µl of substrate solution was added to each well

and incubated for 20 min at room temperature while being protected from light. After this

20 min incubation time, 50 µl of stop solution was added to each well. The optical

density of each well was determined within 30 min using a microplate reader with a

wavelength of 450nm. The reported optical density (OD) readings were corrected by

subtracting the OD reading for the blank well and the pg/ml of each sample was read

from the standards curves.

2.14   Bilayer lipid membrane synthesis

The lipids, 1, 2-diphytanoyl-sn-glycero-3-phosphocholine (DPhPC) and 1, 2-

diphytanoyl-sn-glycero-3-phosphoserine (DPhPS), were purchased from Avanti Polar

Lipids (Alabaster, AL). Bilayer lipid membranes were formed using the Planar Bilayer

Workstation (Black Lipid Membranes, BLM), Warner Instruments, coupled with a stereo

microscope. The work station was comprised of a Faraday cage with vibration isolation

table, Models FC-1 and FC-2, which houses the BLM chamber and the electrical circuitry

　　　　To synthesize a membrane, 2400 µl of potassium chloride (KCl) buffer was added

to each well of the chamber and then a pair of 3 ml syringes was connected to the

chamber wells. These were used to manipulate the buffer volume in each well. The wells

were separated by a Teflon tape. The buffer was lowered below the hole in the Teflon

tape and the stereo microscope was used to ensure that the volume was low enough.

Using a 10 µl capillary tube, 10 µl of the lipid dissolved in pentane was added to the

surface of the buffer in each well. Approximately ~0.5 µl of hexadecane pentane was

then placed over the hole using a pipet tip for delivery. This was done while viewing the

tip through the microscope. 5-7 min after adding the lipid, the buffer was raised above the

hole, by injecting it with the syringes, to form a membrane.
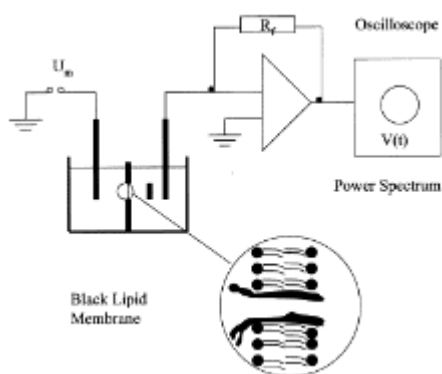
Figure 1. Image showing set-up of the apparatus for the synthesis of the lipid membrane.
Note. Adapted from: *Current Opinion in Colloid & Interface Science,* p. 250-255, by
Winterhalter, (2000).

Fig. 1 shows the basic set-up for the apparatus after the buffer had been raised above the hole. The formation of the membrane within the Teflon tape was detected by the current conductance and voltage readings on the electrical equipment. The oscilloscope was used to assess the presence and stability of a membrane. The Bilayer clamp Amplifier, model BC-535; SUNStir Dual –function controller with SPIN Stirplate and SUN-1 Lamp, model SUNStir-3; and the Low pass Bessel Filter 8 pole (Hamden,CT) were all used to monitor the membrane stability and channel activity. When a stable membrane was formed, the capacitance was noted to be around 100 pF. The current across the membrane ranged from 0 to 2 pA and the voltage was set to zero. The membrane was allowed to stabilize for 10 min, then a voltage of 50 mV or 100 mV was applied to ensure that there was no residue of any channel forming agent, for instance GA, left in the chamber. Without any GA, there should be no significant changes in the current or capacitance of the membrane and the formed membrane would show as a flat line on the pCLAMP 10 Electrophysiology Data Acquisition and Analysis Software. The electrical circuitry along with the pCLAMP 10 software showed graphs generated depicting the status of the membrane activity.

2.15   CNT bilayer lipid membrane protocol

The CNTs were prepared as described in the CNT preparation section, 2.1, and a 200µl volume of CNT-media solution was added to the buffer in the wells. The effect on the membrane was measured for 90 min. A separate study involved the addition of 0.5 µl of 10^{-13} M of the ion channel reporter protein, GA, to each well. The channels were allowed to form and propagate for 30 min, after which a 200µl volume of CNT-media

solution was added to each well. The membrane activity was measured for 90 min and the resultant channel activity was assessed compared to the control.

CHAPTER 3. RESULTS

3.1   Characterization of carbon nanotubes

3.1.1   Zeta potential

When a particle enters a new liquid medium, a net charge develops at its surface

due to the distribution of ions and oppositely charged ions. First, there is the development

of a layer of strongly bound counterions, the stern layer; secondly, a diffuse layer of

positive and negative ions, which are less firmly attached, orient themselves around the

stern layer. Within the diffuse layer there is a boundary where the ions form a stable

conformation which travels along with the particle, whereas ions beyond this boundary

are unaffected by the particle's movement. This boundary is called the slipping plane,

and the potential within this region is the zeta potential.
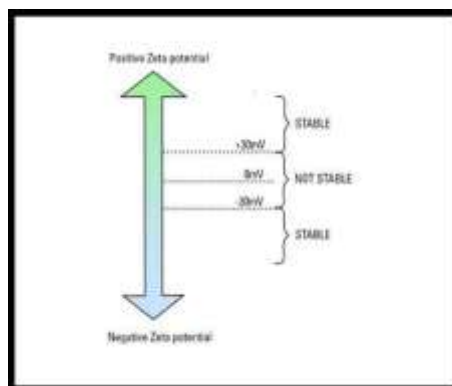
Figure 2: Zeta potential values can be negative or positive. Values that are more negative
than -30 mV or more positive than +30 mV indicate that the measured particles are more
likely to form a uniform colloid system. Values within the range of -30 mV and +30 mV

The magnitude of the zeta potential indicates how stable a colloid system is, and the likelihood that the individual particles may repel each other or agglomerate. Fig. 2 illustrates that the particles within the region of -30mV to 30mV are considered to have low zeta potential values and therefore will submit to the influence of their surface charges, attract each other, and flocculate. Particles with zeta potential values beyond this range tend to form stable colloid systems. They remain evenly dispersed in solution and therefore repel each other due to their large surface charges.

Zeta potential measurements were done on short and long CNTs to assess their agglomerating potential in cell culture media. The CNTs were all non-functionalized and were prepared and used without further physical or chemical modifications. The method of preparation of the CNTs is described in section 2.1.

Table 1 shows the zeta potential values for the short MWCNT concentrations ranging from 100 µg/ml to 100 pg/ml. There was an average zeta potential of -7.85 mV. Since this average fell within the -30 mV and +30 mV range, these data indicate that the nanotubes have a great potential to agglomerate. The agglomerating potential of the nanotubes indicate that they could impose a micro or nano effect, depending on what they may be interacting with. Larger agglomerates may function as single units and could cover smaller cells in a biological environment and therefore have a micro effect. However, smaller dispersed nanotube bundles may affect a single protein or interact with the cell membrane and therefore have a nano effect.

Table 1: Zeta potential measurements for short raw and pristine MWCNTs which were prepared in cell culture media. The zeta potential values were from -7.5 and -10.2 mV. * indicates the outlier value 0.02 mV.

Concentration	Short MWCNT	
µg/ml	Purified (mV)	Original (mV)
100	-8.6	*
10	-7.8	-9.1
1	-9.7	-7.5
0.1	-10.2	-8.6
0.01	-9.2	-8.8
0.001	-8.9	-7.5
0.0001	-8.0	-8.3
Control	-7.6	

Table 2: Zeta potential measurements for long SW and MW CNTs which were prepared in cell culture media. Measurements ranged from -3.0 mV to -9.9 mV. *Note*. Adapted from: *Cellular Physiology and Biochemistry*, p. 197-212, by Banga, Witzmann, Petrache & Blazer-Yost, (2012).

Concentration	Long CNT	
µg/ml	Single-wall (mV)	Multi-wall (mV)
100	-8.9	-3.0
10	-8.5	-6.7
1	-5.0	-7.2
0.1	-5.5	-7.0
0.01	-9.9	-4.6

Table 2: continued.

0.001	-6.7	-7.2
0.0001	-8.6	-7.2
Control	-4.7	

Table 2 shows that the zeta potential measurements for the long SW and MW

CNTs were all within the -30 mV and 30 mV range, indicating that these CNTs have the

potential to agglomerate. The cell culture media contained FBS. The similarity in zeta

potential values of the control and the experimental samples indicated that the proteins in

the media and the CNTs might be interacting to form complexes that have physical

properties similar to that of serum proteins. Davis, (1998) and Kam and Dai, (2005)

showed that proteins may become conjugated with nanotubes in various ways: two of

which are by direct surface adsorption of proteins to nanotubes or encapsulation of the

proteins by the nanotubes.

In order to address the question of the interaction between the protein and CNTs,

short MWCNT and long SWCNT samples were prepared with cell culture media in order

to image the CNT-protein and CNT-CNT complexes, which were formed in solution, by

using a transmission electron microscope.

Figs. 3a and 3b show the samples of CNTs that were prepared in serum free

media. Fig. 3a shows large clumps of agglomerated nanotubes. The magnified image of

Fig. 3a shows one of the regions where the nanotubes formed bundles by aligning

themselves next to each other. These bundles also joined each other to form longer chains.

The measurement of the diameter of one bundle at the top of the image is 28.6nm. This

value is less than the value that was reported by the manufacturers. MWCNTs were

reported to have diameters of 40-60 nm. These data indicated that these particles may

have been broken down by the sonication step during the sample preparation. Kosynkin

et al. (2009) and his group illustrated that the sonication process has the potential to cut

SWCNTs. Sonication caused some shortening of their nanotubes making them more

suitable for Scanning Electron Microscope (SEM) imaging.

3.1.2   Transmission electron microscopy
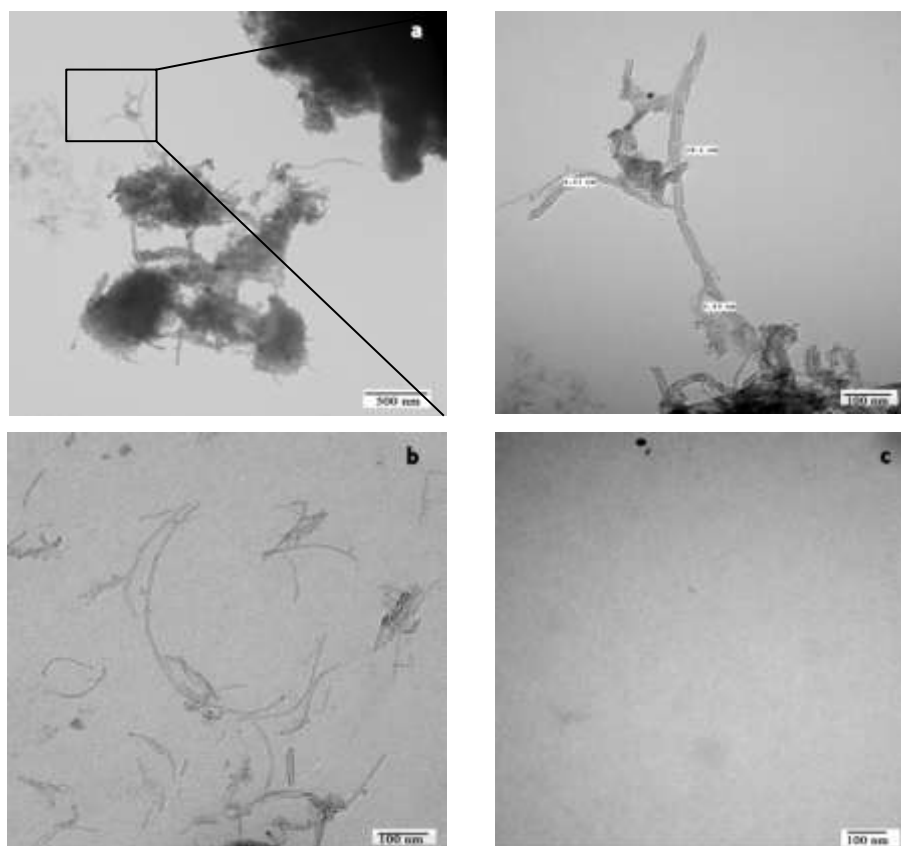
Figure 3: Transmission electron micrographs showing the agglomeration pattern of short pristine MWCNTs dissolved in serum free media. The NP solutions were incubated for 48hrs on formvar carbon film on 400 mesh copper (FCF400-Cu) grids. (A). High concentrations, 4μg/cm^2, of nanotubes. The image on the right shows a higher magnification for the marked area. (B). Medium concentrations, 4ng/cm^2, of nanotubes. (C) The control sample contained only serum free media.

Fig. 3b shows many nanotube fragments which resulted from the prepared samples. Compared to the 100 nm scale on the bottom right corner of the image, many nanotube fragments were shorter than the manufacturer reported lengths of 1-5 μm. Sonication is a critical step which is done to ensure the even distribution of the nanotubes in solution. The experimental and control samples were sonicated for 20 pulses, while a separate vial, with a volume of FBS equal to the volume of the experimental vials, was

sonicated for 10 pulses between samples, in order to coat the sonication probe. Fig. 3c shows the result of the control for the serum free media samples. This control contained only serum free media which was made with 1 packet of DMEM/F-12, 1mM glutamax, 0.4% penicillin/streptomycin and 2.4g/L $NaHCO_3$.

The serum protein supplies the cells with growth factors and hormones, binding and transport proteins, additional amino acids, vitamins and trace elements, as well as protease inhibitors (Gstraunthaler & Gerhard, 2003). Therefore, it is a critical component in the cell culture media. 15% and 5% FBS is used in the cell culture media preparation of the Calu-3 cell line and T84 cell line, respectively. However, in preparing the samples for TEM imaging, only 2% FBS was used in the media, in order for the nanotubes to be better seen in the microscope image. Fig. 4 shows samples prepared with 2% FBS media. The nanotubes are not visible, but the apparent elongated and clumped structures appear to be nanotubes covered in serum proteins. The elongated structures are seen in Figs. 4a and 4b but in Fig. 4c there are smaller globules. Lynch et al., (2007) explained that the CNTs often form complexes with proteins rendering the nanotubes more biologically active.
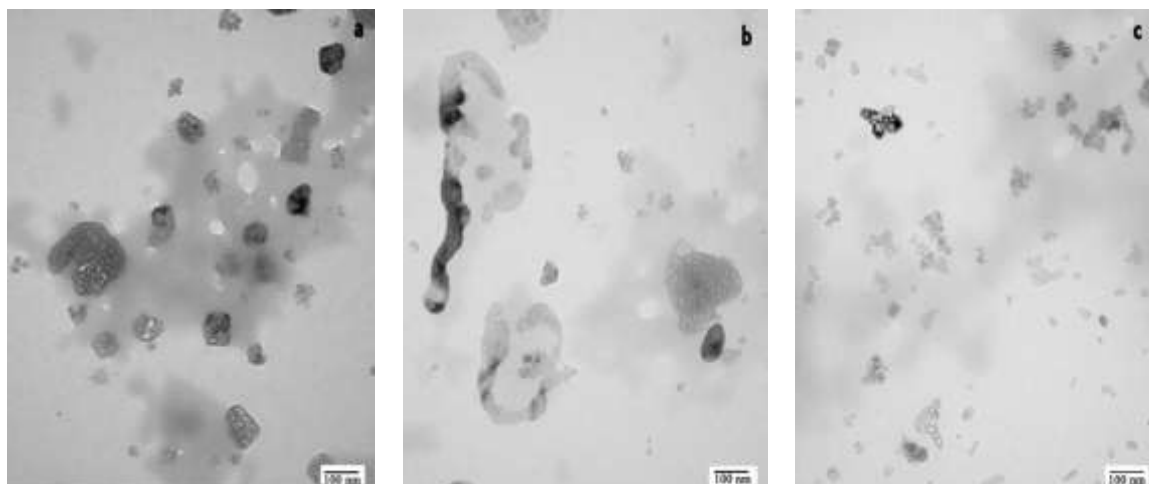
Figure 4: TEM images showing the agglomeration pattern of short pristine multi-walled CNTs dissolved in 2% FBS- supplemented cell culture media. The NPs were incubated for 48hrs on formvar carbon film on 400 mesh copper (FCF400-Cu) grids. (A) High concentration- $4\mu g/cm^2$, of nanotubes. (B) Medium concentration- $4ng/cm^2$, of nanotubes. (C) The control sample contained only serum free media.

The following image, Fig. 5, shows TEM images of the long SWCNTs. These

nanotubes show similar fragmentation and bundling of the short MWCNTs, but there was

no apparent uniformed arrangement. The thick black region at the top of Fig. 5a shows a

mass of highly agglomerated nanotubes. The magnified image of Fig. 5a shows a

nanotube bundle protruding from this mass. These data illustrate the magnitude of

agglomeration that occurs with the high concentration of nanotubes, $4\mu g/cm^2$. Fig 5b is

the control which had only serum free media. The spots on the left and right margins of

the images may be due to sample artifacts.
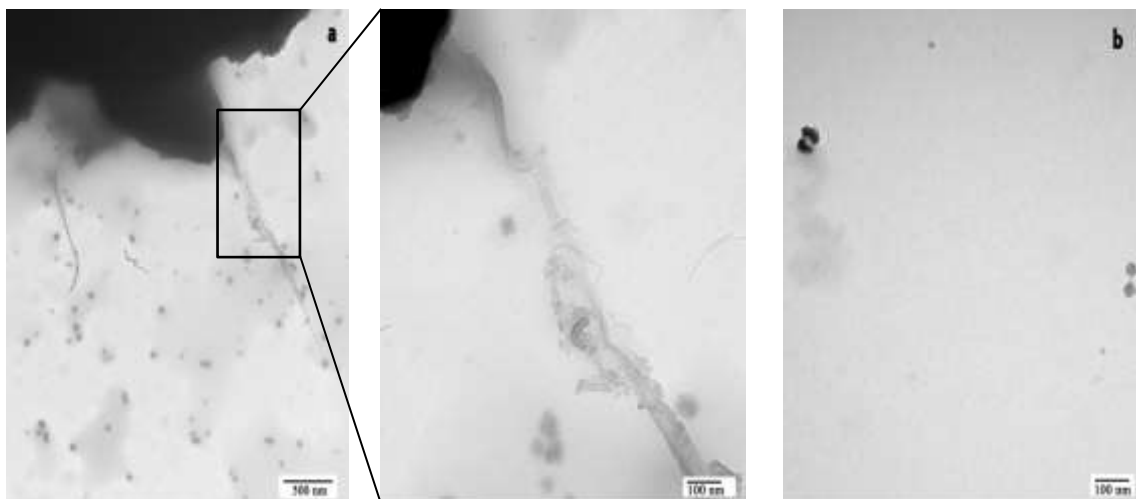
Figure 5: TEM images showing the agglomeration pattern of long pristine single- walled CNTs dissolved in Serum free media. The NPs were incubated for 48hrs on formvar carbon film on 300 mesh Nickel (FCF300-Ni) grids. (A). High concentration, $4\mu g/cm^2$, of nanotubes. (B). Control sample contained only serum free media.
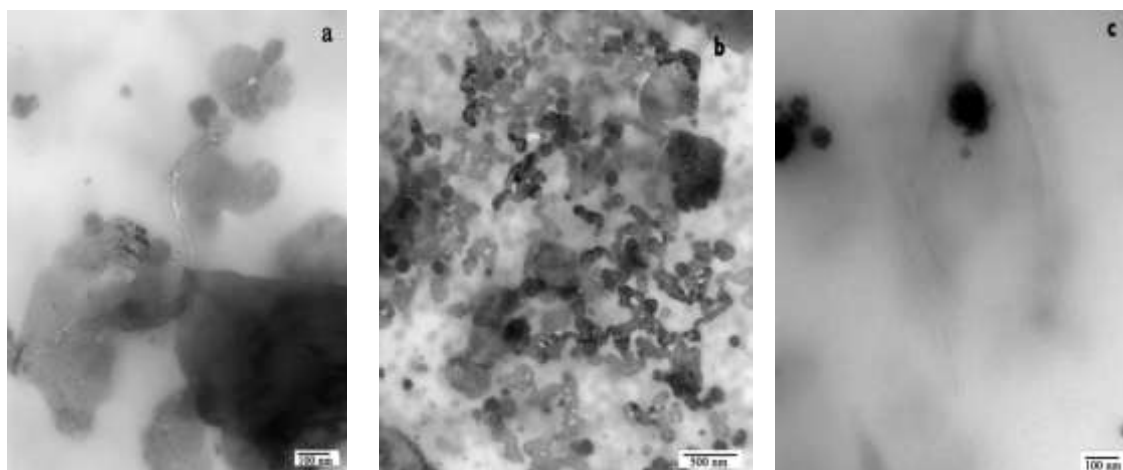
Figure 6: TEM images showing the agglomeration pattern of long pristine single-walled CNTs dissolved in 2% FBS cell culture media. The NPs were incubated for 48hrs on formvar carbon film on 400 mesh Nickel (FCF300-Ni) grids. (A). High concentration- $4\mu g/cm^2$, of nanotubes. (B). Medium concentration- $4ng/cm^2$, of nanotubes (C) The control sample contained only 2% FBS media.

Fig. 6 shows the TEM images of the long SWCNTs that were prepared in 2%

FBS cell culture media. Fig. 6a shows one nanotube that is not completely surrounded by

the proteins, and they are adsorbed to it along its length. Fig. 6b shows many cylindrically shaped structures which may be nanotube fragments covered by proteins.

The images also show that CNTs formed micro or nano structures based on the concentration of the CNT sample. The nanotube concentrations which may come into contact with humans vary. They generally come into contact with the epithelial linings of our skin, lungs or digestive tract. Krug and Wick, (2011) assert that the lungs are the main portal or entry by which nanotubes come into contact with the human body among the other routes. Therefore, a dose response study was conducted using the Calu-3 line to simulate the effect of long MWCNTs, of physiologically relevant concentrations, on human airway epithelial cells. First the Calu-3 cell line was characterized to determine its physiological similarity to the lung epithelial tissue.

3.2   Characterization of the calu-3 cell line

3.2.1   Hormonal secretion and inhibition
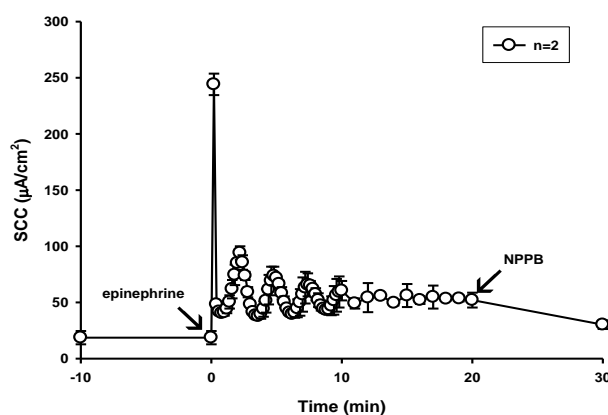
Figure 7: Calu-3 cells were grown to a confluent monolayer on Transwell polycarbonate permeable membranes for 14 days. The data shows the effect of epinephrine (10^{-6} M) stimulation, added at time = 0 min, followed by NPPB (100 µM), which was added at time = 20 min to inhibit the chloride secretion. *Note*. Adapted from: *Cellular Physiology and Biochemistry*, p. 197-212, by Banga, Witzmann, Petrache & Blazer-Yost, (2012).

Calu-3 cells became confluent and formed high resistance epithelia within 14 days on Costar-Corning Transwell polycarbonate permeable membranes. These membranes were then cut out from the Transwell inserts and mounted unto Ussing chambers in order to measure their TEER and SCC by electrophysiology, as described in section 2.7.

Epinephrine stimulates the secretion of Cl^- ions via the cAMP/PKA pathway. It is a beta agonist that binds to its serosal surface receptor (Sprague et al., 2001). This surface receptor in turn activates Adenylyl cyclase (AC). AC catalyzes the conversion of ATP to cAMP. The released cAMP binds to protein kinase A (PKA) to expose its active site. Kinase-A, in turn, phosphorylates the chloride channel CFTR to allow apical chloride secretion (Meinkoth, 1993 & Egan, 1992). Fig. 7 shows that the stimulation of the Calu-3 cells with epinephrine produces a characteristic large initial peak which is followed by a series of dampening oscillations. The addition of NPPB, a general Cl^- and K^+ channel inhibitor, at time 20 min post stimulation, resulted in a decrease in the SCC indicating that the remaining SCC was partially due to chloride secretion.

The second effector used was Forskolin. It stimulates adenylyl cyclase (AC) directly, and in turn, it induces an increase in cAMP levels. After further stimulation of the forskolin-pretreated cells with epinephrine, the amplitudes were still smaller than the control amplitudes. Forskolin also failed to fully stimulate the initial Cl^- peak, which was lower in the forskolin stimulated cells, but it was the dominant peak in the control cells.

Epinephrine and forskolin are both able to stimulate the increases in cAMP, and therefore they in turn, induce an increase in SCC levels, by increasing Cl^- secretion in the

Calu-3 cell line. These data indicate that epinephrine may activate additional chloride
channels in the Calu-3 cell line that may not be responsive to forskolin.
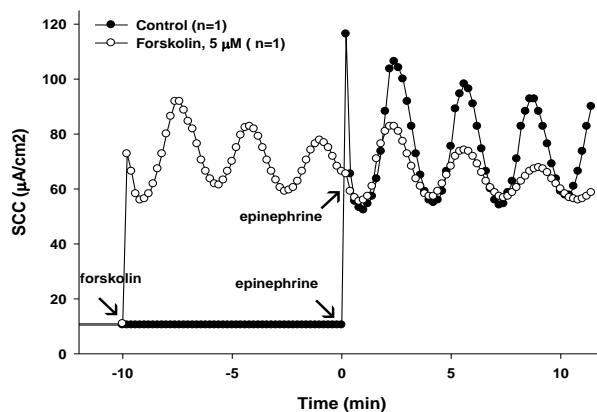
Figure 8: Calu-3 cells were grown to a confluent monolayer on Transwell polycarbonate permeable membranes for 14 days. Cells response to epinephrine (10^{-6} M) stimulation, time = 0 min, after pretreatment with forskolin (5 μM) which was added at time = -10 min.
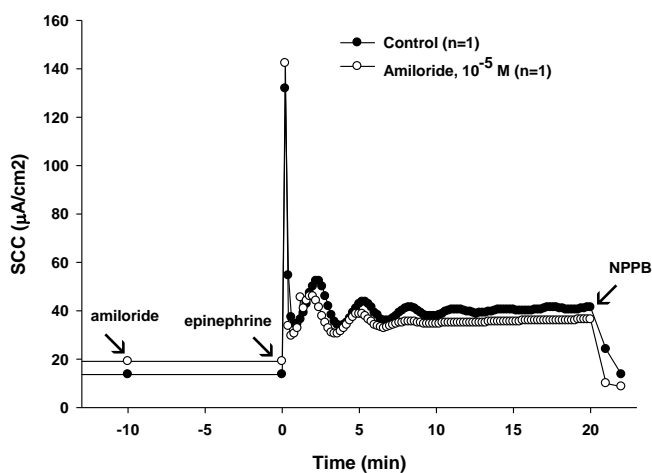
Figure 9: Calu-3 cells were grown to a confluent monolayer on Transwell polycarbonate permeable membranes for 14 days. The cells were pretreated with amiloride (10^{-5} M) at time = -10 min followed by stimulation with epinephrine (10^{-6} M) at time = 0 min. NPPB (100 μM) was added at time = 20 min to inhibit the Cl⁻ secretion.

Electrophysiology measurements were further done to confirm whether Calu-3 the cell line contained any epithelial sodium channels (ENaC). Amiloride is a specific inhibitor of ENaC; therefore, inhibiting this channel blocks the sodium absorption in the cells. An increase in SCC is due to the secretion of negatively charged ions or absorption of positively charged ions. Fig. 9 shows that there was no change in the baseline when amiloride was added at time = -10 min indicating that the baseline current was not due to sodium ion absorption. The peak which was generated when epinephrine was added at time = 0 min was not altered by amiloride pretreatment. This indicates that the stimulated SCC was also not due to sodium ion absorption.

LY294002 is an inhibitor for phosphatidylinositol 3-kinase (PI3 kinase). Păunescu, Blazer-Yost, Vlahos, and Helman, (2000) showed that PI 3-kinase is required for insulin-mediated Na$^+$ reabsorption via ENaC in the renal, A6 cell line. Hence inhibition of PI 3-kinase with LY294002 will cause a reduction in the density of open ENaC in the apical membrane of the cells. It will thereby reduce Na$^+$ absorption. Previous data showed that the Calu-3 cell line does not contain ENaC; therefore, our data in Fig. 10a is consistent with these findings, in that the baseline and stimulated SCC were not significantly affected by the LY294002 inhibitor. While other studies show that the Calu-3 cell line does contain ENaC, the lack of this channel in our batch of cells may be due to the loss of the functioning of this channel over many passages. Kunzelmann, Kathöfer, Hipper, Gruenert, and Greger (1996) showed that the T84 cell line lost their sodium absorptive capacity over time due to cell culturing. Upon addition of the inhibitor there was a slight increase in the baseline SCC which is further increased upon stimulation with epinephrine at time = 0 min.

Figure 10: Calu-3 cells were grown to a confluent monolayer on Transwell polycarbonate permeable membranes for 14 days. (A) Cells' response to LY294 002 (B) Response to LY294 002 coupled with CFTR inh-172. The inhibitors were added at time = -10 min followed by epinephrine (10^{-6} M) stimulation, time = 0 min.

Komalavilas et al. (2001) showed that treatment of vascular smooth muscle with LY294002 caused an increase in the activity of cAMP-dependent protein kinase and phosphorylation of the cAMP-dependent protein substrate heat shock protein 20. A

schematic representation of the regulation of vascular smooth muscle by PI-3 kinase showed that, PI 3-kinase was blocked with LY294002, and there was an accumulation of cAMP in cells. These data show that the inhibitor may have a partial stimulatory effect on the cell line. Epinephrine stimulation induced a marked increase in SCC compared to the baseline. The height of the experimental peak is similar to that of the control cells which were stimulated by only epinephrine.

In Fig.10b there was a decrease in baseline once the PI3 kinase inhibitor was added along with the CFTRinh-172. This showed that the baseline current was partially due to Cl^- secretion via CFTR. Further stimulation with epinephrine at time = 0 min resulted in no stimulation beyond the baseline. These data further confirmed that the stimulated SCC current was largely due to Cl^- secretion.

U73122 is an aminosteroid which functions as an inhibitor of phospholipase C. It also works by depleting intracellular calcium stores (Mogami, Mills, & Gallacher, 1997). In Fig. 11a when U73122 was added at time = -10 min there was no change in the baseline. This data suggested that the baseline current may not be influenced by this inhibitor. Following the inhibition, there was an increase in the stimulated SCC peak after epinephrine was added at time = 0 min. Fig. 11b shows that there was no decrease in the baseline after pretreatment with U73122 and CFTR inh-172, but there was a decrease in SCC after stimulation with epinephrine. While these data showed that U73122 failed to dampen the stimulated SCC, in the presence of the CFTR inhibitor the current was decreased. This indicated that CFTR plays a major role in the stimulated SCC.
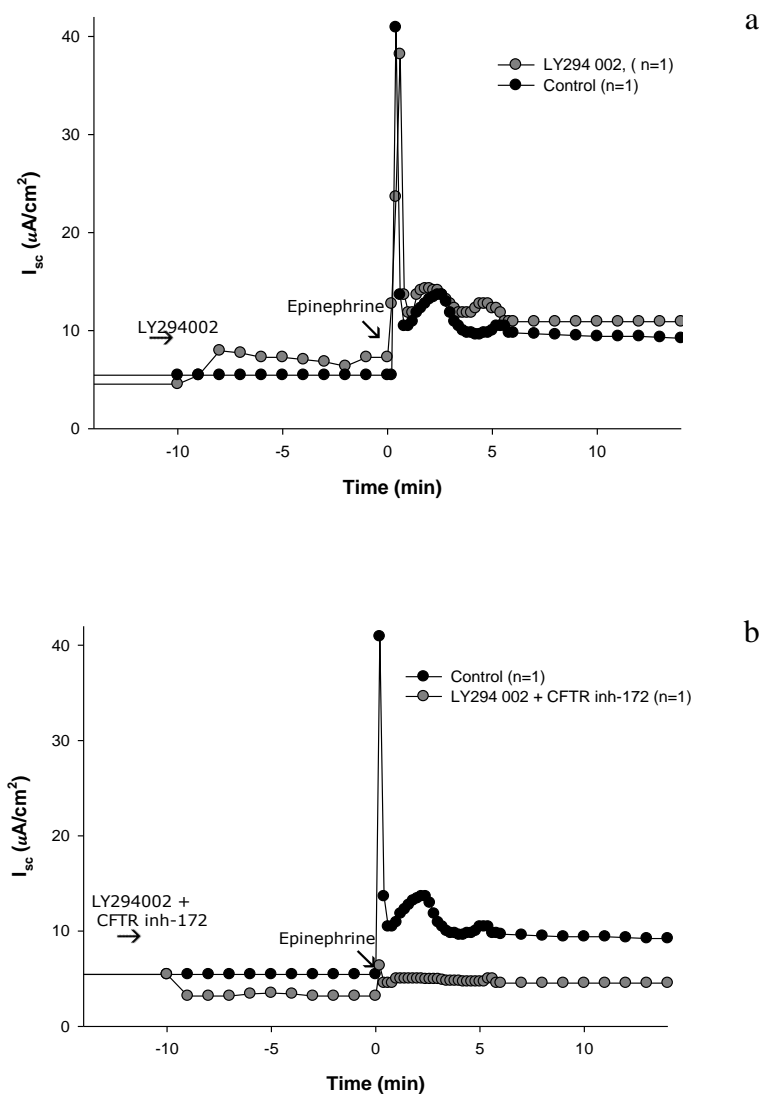
Figure 11: Calu-3 cells were grown to a confluent monolayer on Transwell polycarbonate permeable membranes for 14 days. (A) Calu-3 cells response to the stimulation with epinephrine (10^{-6} M) which was added at time = 0 min, after pretreatment with U73122. (B) Pretreatment with U73122 coupled with CFTR inh -172 which was added at time = -10 min.
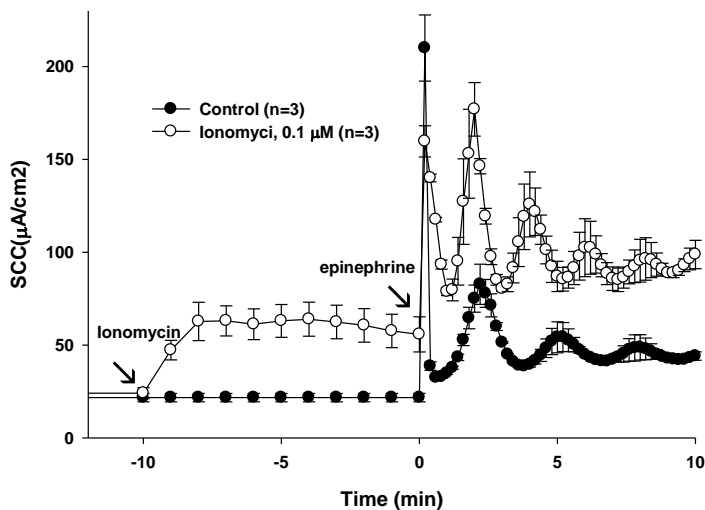
Figure 12: Calu-3 cells were grown to a confluent monolayer on Transwell polycarbonate permeable membranes for 14 days The Calu- 3 cell response to pretreatment with ionomycin (0.1μM) which was added at time = -10 min, followed by the stimulation with epinephrine (10^{-6} M) at time = 0 min.

Ionomycin is a calcium ionophore which elevates intracellular calcium levels (Klaus et al., 2005). Cells were pretreated for 10 min, followed by stimulation with 10^{-6}M epinephrine at time = 0 min. This resulted in an initial elevation in basal SCC. After further stimulating with epinephrine, there was a slightly smaller initial peak followed by a series of dampening oscillations with a higher basal ion flux compared to the control. These data suggest that the initial peak is strongly influenced by CFTR and the following peaks are influenced by both CFTR and a CaCC.
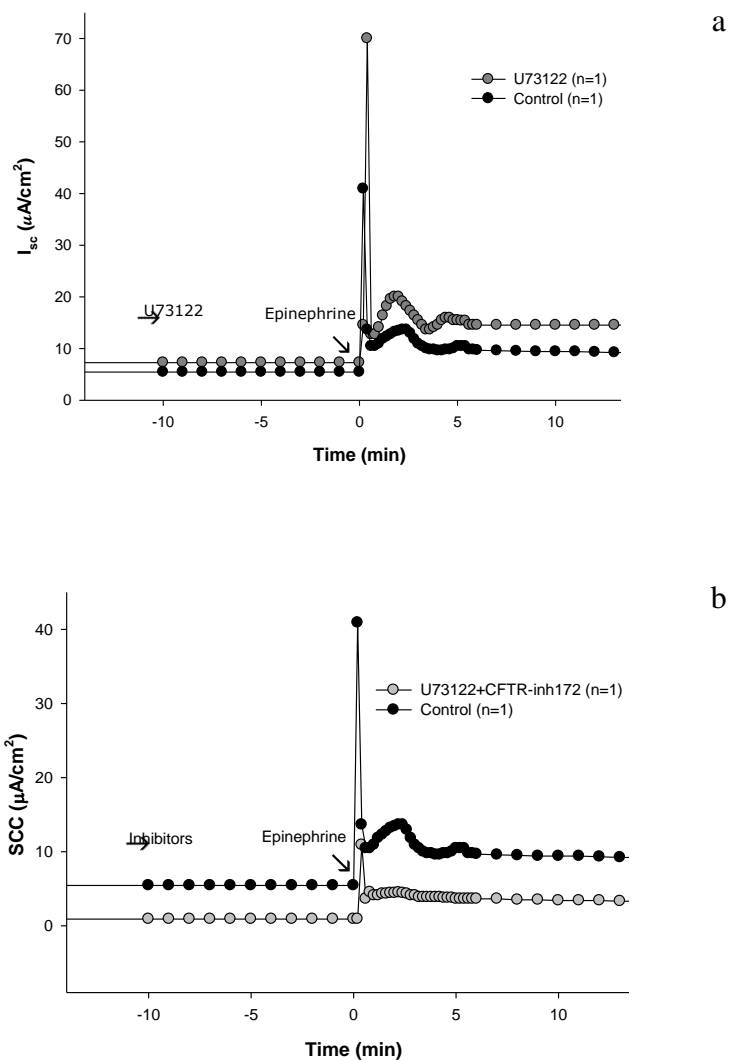
a

b

Figure 13: Calu-3 cells were grown to a confluent monolayer on Transwell polycarbonate permeable membranes for 14 days. (A) Cell response to epinephrine (10^{-6} M) after pretreatment with BAPTA-AM (100μM) added at time = -10 min. (B) This magnified graph shows the changes in baseline current during the first 10 min prior to epinephrine stimulation. The first peak of the BAPTA-AM pretreated cells was significantly different from that of the control, P= <0.001.

1,2-bis(2-amino phenoxy)ethane-N,N,N,N-tetraacetic acid–tetrakis

(acetoxymethyl ester) (BAPTA –AM) is a membrane permeant calcium chelator (Chen

et al., 2002). The addition of BAPTA-AM at time = -10 min caused a decrease in free

intracellular calcium. The mean value of the initial peak of the control cells (M =123.64,

SD=10.33) was significantly higher than that of the BAPTA-AM pretreated cells (*M* =31.21, *SD*=11.412), *p*=< 0.001. Upon addition of the ester there is a decrease in SCC to below baseline time = -3 min to time = 0 min. Stimulation with epinephrine produced a small initial peak and a smaller second peak with a following flat line. These data indicate that BAPTA-AM's action inhibited basal current and it failed to inhibit all the Cl⁻ secretion in the cell, indicating that not all the chloride secretion is dependent on Ca^{+2}, Fig. 13.

CFTR inh-172 is the inhibitor for CFTR (Ma et al., 2002). The Calu-3 cells were pretreated with the inhibitor, and this caused a significant decrease in the initial chloride peaks after epinephrine stimulation at time = 0 min. The peak of the control cells (*M* =77.27, *SD*=14.35) was significantly larger than that of the CFTR inh-172 pretreated cells (*M* =21.02, *SD*=4.05). These data indicate that Calu-3 Cl⁻ secretion is due, in part, to the CFTR channel, Fig. 14

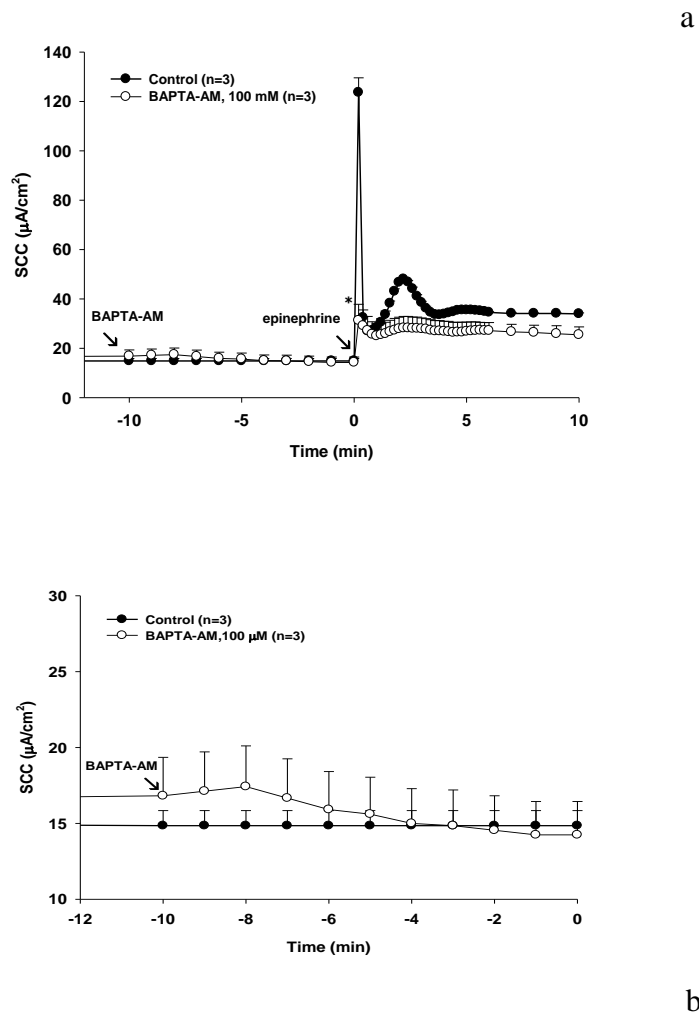**Figure 14:** Calu-3 cells were grown to a confluent monolayer on Transwell polycarbonate permeable membranes for 14 days. Epinephrine-stimulated (10^{-6} M), cells response to the pretreatment with CFTR inh-172 (10μM) added at time = -10 min, followed by epinephrine at time = 0 min. The first peak of the CFTR inh-172 pretreated cells was significantly different from that of the control, P= <0.001.
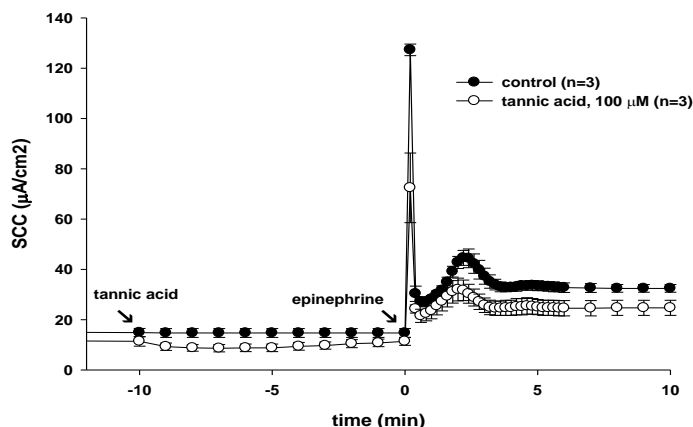
Figure 15: Calu-3 cells were grown to a confluent monolayer on permeable transwell membranes for 14 days. The cell response to tannic acid (100µM) which was added at time = -10 min, followed by epinephrine (10^{-6} M) which was added at time = 0 min. The first peak of the tannic acid pretreated cells was significantly different from that of the control, P= 0.017.

Tannic acid is a specific inhibitor for the transmembrane ion transporter (TMEM16A), a calcium activated chloride channel (CaCC), whereas the CFTR chloride channel is unaffected by it (Namkunj et al., 2010). When tannic acid was added at time = -10 min, there was a decrease in the baseline current, and after epinephrine stimulation, tannic acid inhibited approximately half of the total initial peak. The initial peak of the epinephrine stimulated control cells (Mean, M =127.273, Standard Deviation, SD=3.963) was significantly larger than that of the tannic acid pretreated cells (M =72.424, SD=23.95). This indicated that CaCC secretion via TMEM-16a partially contributed to the baseline current and stimulated total chloride secretion, Fig. 15.

Fig. 16 shows the result of the Calu-3 cell line pretreatment with tannic acid plus CFTR inh-172. The coupled inhibitors induced a small transient peak. This showed that the two inhibitors had a short-lived stimulatory effect on the Calu-3 cell's chloride

channels. This was followed by a decline in the baseline SCC, indicating that the baseline current was due to chloride secretion via CFTR and TMEM-16a. Fig. 16b shows an enhanced peak for the first twelve min after pretreating the cells with both inhibitors. The difference in the median values between the baseline of the control and experimental groups was statistically significant. There was a difference in the groups from time = -4 to time = 0 min, p = 0.005. However, the experimental initial peak (*M* =23.49, *SD*=7.39), which was generated due to the stimulation with epinephrine, was significantly different from the control initial peak (*M* =110.30, *SD*=44.11).The difference in the mean values of the two groups was greater than would be expected by chance (*p*= 0.028). These data indicated that the total SCC was due to chloride ion secretion.

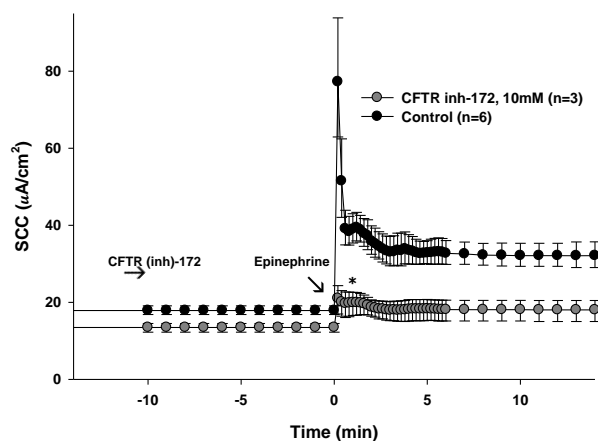a   b
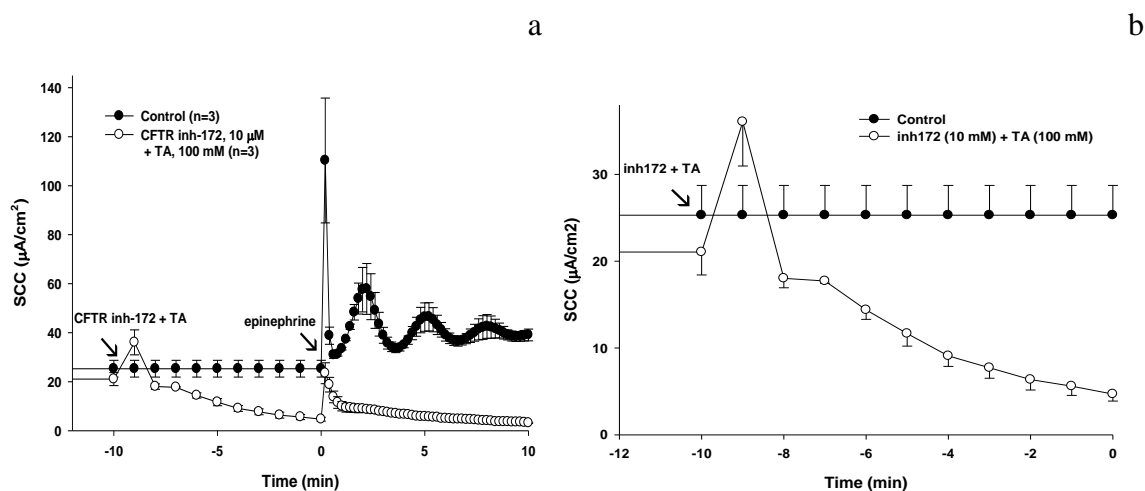
Figure 16: Calu-3 cells were grown to a confluent monolayer on Transwell polycarbonate permeable membranes for 14 days. (A) Cell line response to tannic acid (100μM) and CFTRinh 172 (10μ M) pretreatment which was added at time = -10 min, followed by epinephrine (10^{-6} M) stimulation at time = 0 min. Graph shows the first 10 min of the effect on the cell line. (B) The first effect of the inhibitors during the first 12 min prior to epinephrine stimulation.

3.2.2 Fluid secretion
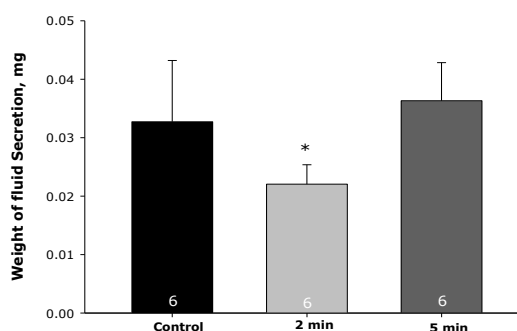
Figure 17: Calu-3 cells were grown to a confluent monolayer on Transwell polycarbonate permeable membranes for 14 days. The apical media was removed and then cells were stimulated with epinephrine (10^{-6} M) for 2 min and 5 min. The experimental bars (n=6) were not significantly different from that of the non- stimulated, control cells (n= 6). * indicates that the mean values for the 2 min and 5 min experimental groups where significantly different, p=0.003.

Figure 18: Calu-3 cells were grown to a confluent monolayer on Transwell polycarbonate permeable membranes for 14 days. The cells were stimulated with epinephrine (10^{-6} M) without removing the apical media for 2 min and 5 min. The total fluid secretion volume was weighed. Experimental bars (n = 8) were not statistically significant from that of the control (n = 8), *p*= 0.375).

Further assessment was done to determine whether epinephrine stimulated Cl⁻ induced apical fluid secretion in the Calu-3 cell line. The Calu-3 cells were basolaterally stimulated for 2 min and 5 min and then their apical fluid secretion weights were compared to that of the control, non-stimulated cells. Fig. 17 shows the mean fluid secretion weights of the cells which were stimulated after first removing the apical fluid. The results of a One-Way ANOVA shows that epinephrine significantly changed the apical fluid secretion weights of the Calu-3 cells, $F = (2, 15) = 4.042$, $p = 0.04$. There was a larger apical secretion weight from the cells stimulated for 5 min ($M = 0.0363$, $SD = 0.00798$) than from those stimulated for 2 min ($M = 0.022$, $SD = 0.00405$). This

indicated that the secretion volume was proportional to the length of the stimulation time. An independent samples Student's t-test showed that there were significant differences between the 2 min and the 5 min experimental mean values, t (10) = -3.904, p = 0.003. The experimental bars were not statistically different from the control.

Fig. 18 shows the mean fluid secretion weights of the cells that were stimulated without first removing the apical fluid secretion. The results of a One-Way ANOVA shows that epinephrine did not significantly affect the apical fluid secretion weights of the cells, F= (2, 21) = 0.531, p=0.6. There was no significant difference in apical fluid secretion between the 2 min experimental group (M=0.73, SD=0.12) and the 5 min experimental group (M=0.78, SD=0.08), p = 0.375.

Calu-3 cells were cultured without any apical media in order to simulate the physiological air-liquid (AL) interface as described in the *Methods* section 2.5. The cells were able to secrete their own apical fluids to keep from drying up. Fig. 16 shows, that before the cells were stimulated, there was a baseline current indicating that there was constant chloride ion secretion in the absence of hormonal influence. This baseline current was decreased by inhibiting the Cl⁻ channels and was elevated by stimulation of Cl⁻ channels with epinephrine (10^{-6} M).

In the first experiment Fig. 17, the apical fluid secretion was removed before stimulating the cells, so that the total fluid secretion measured would only be due to the influence of epinephrine. In the second experiment, Fig. 18, the cells were stimulated without removing the apical fluid secretion. This was done so that the cells would be stimulated without first changing their immediate environment by the removal of the apical media.

In order to confirm the cAMP – dependent Cl$^-$ secretions, we tested for the presence and levels of cAMP using an ELISA kit. Calu-3 cells were grown to confluence and then stimulated with epinephrine (10^{-6} M) for 20 seconds and 1 min on the Transwell polycarbonate permeable membranes. Epinephrine caused increases in cAMP due to the stimulation of the epinephrine adrenergic receptor which in turn activated AC to catalyze the conversion of ATP to cAMP.

A Students' t-test shows that there was no significant differences between the 20 s epinephrine stimulated cells' (*M*=63.0, *SD*=41.9), *p*= 0.137 or the 1 min epinephrine stimulated cells' (M=77.9 SD=57) p= 0.167 with control cells (*M*=4.71, *SD*=2.61). The histogram showed that there was a difference between the control and the experimental samples but the lack of significant difference may be due to the large standard error values, Fig. 19. A larger sample size may result in a significant difference.

Characterized Calu-3 cells were used to measure the effects of carbon NPs on TEER and SCC. The following dose response data showing the effects of SWCNTs and MWCNTs were generated and published by Banga et al., (2012).
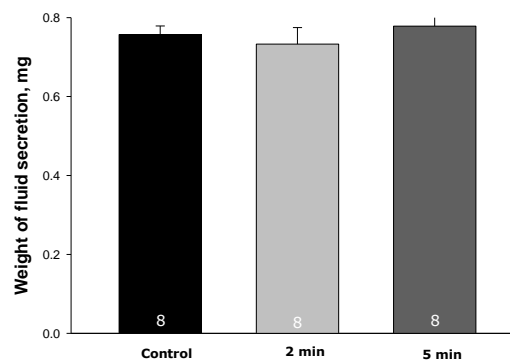
3.2.3   cAMP levels in calu-3 cells
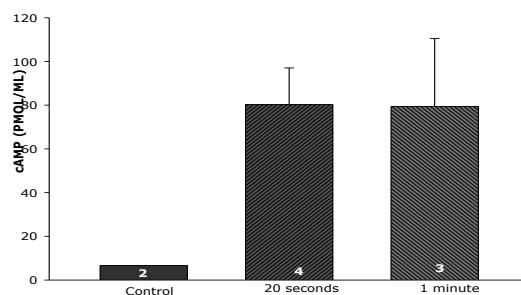
Figure 19: Calu-3 cells were grown to a confluent monolayer on Transwell polycarbonate permeable membranes for 14 days. Cells were stimulated with epinephrine (10^{-6} M) for 20 s and 1 min. The increase in cAMP after 20 second and 1 minute stimulations with epinephrine were not shown to be statistically different from the control. The number of replicate experiments performed for each time point is indicated as the values in the bars.

3.3   Dose response of calu-3 cells

a   b
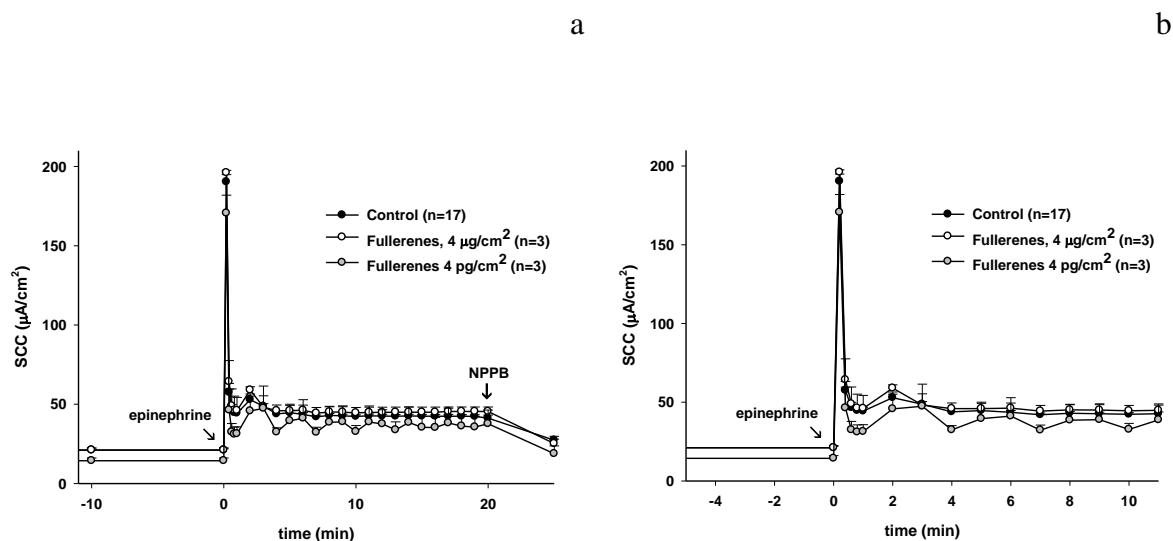
Figure 20: Calu-3 cells were grown to a confluent monolayer on Transwell polycarbonate permeable membranes for 14 days. (A) Cells response to epinephrine stimulation after incubation with the highest concentration (4 μg/cm^2), and lowest concentration (4 pg/cm^2) of fullerenes for 48 h. (B) The first 10 min of the Cl$^-$ secretory phase. There is not a statistically significant difference between the mean values for the initial peak of the control and fulllerene treated groups, *p* = 0.086. *Note*. Adapted from: *Cellular Physiology and Biochemistry*, p. 197-212, by Banga, Witzmann, Petrache & Blazer-Yost, (2012).

Calu-3 cells were grown to confluence and then incubated with the fullerene,

SWCNTs or MWCNTs for 48 h, after which the cells were mounted unto Ussing

chambers for electrophysiology measurements. Epinephrine was added to the cells after

the cells had stabilized, time = 0 min. The epinephrine-stimulated chloride peaks of the

control were nearly identical to the peaks of the fullerene pre-incubated cells, $4\mu g/cm^2$

and $4pg/cm^2$ peaks, Fig. 20.

a   b

Figure 21: Calu-3 cells were grown to a confluent monolayer on Transwell polycarbonate permeable membranes for 14 days. (A) Cells response to epinephrine (10^{-6} M) stimulation after incubation with the highest ($40\mu g/cm^2$) and lowest ($40pg/cm^2$) concentration of SWCNTs for 48h. (B) The enhanced peak showing the first 10 min of the Cl^- secretory phase. There was a significant decrease in the initial peaks, *p*= 0.016. *Note*. Adapted from: *Cellular Physiology and Biochemistry*, p. 197-212, by Banga, Witzmann, Petrache & Blazer-Yost, (2012).

In contrast to the lack of effect after incubation with fullerenes, a Student t-test showed

there was a significant decrease in the initial chloride peaks in the cells incubated with

the high and low concentrations of SWCNTs, $4\mu g/cm^2$ and $40pg/cm^2$ respectively, Fig 21.

Blazer-Yost et al. (2011) illustrated using atomic force microscopy (AFM) that high

doses of CNTs, 40µg/cm^2, agglomerate and therefore these samples have a high

roughness factor (Ra). Alternatively, the low dose samples were highly dispersed as

indicated by a low Ra.
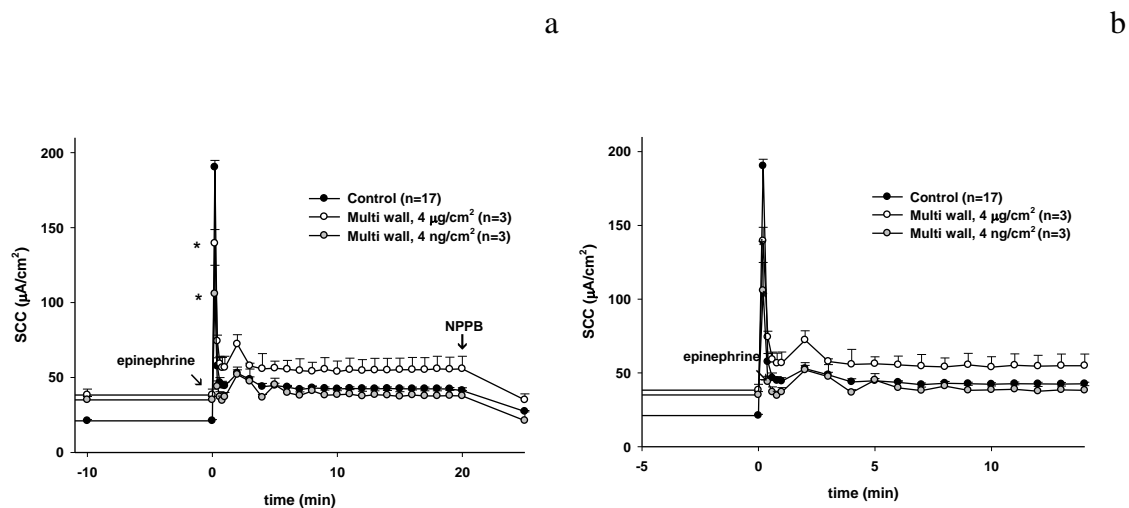
Figure 22: Calu-3 cells were grown to a confluent monolayer on Transwell
polycarbonate permeable membranes for 14 days. (A) Cells response to epinephrine
stimulation after incubation for 48 h with the highest concentration (4µg/cm^2) and lowest
concentration (4ng/cm^2) of MWCNTs. (B) The first 10 min of the Cl$^-$ secretory phase.
There was a statistically significant difference between the CNT treated cells and the
control, $p = 0.016$. *Note*. Adapted from: *Cellular Physiology and Biochemistry*, p. 197-
212, by Banga, Witzmann, Petrache & Blazer-Yost, (2012).

MWCNT exposure also caused a decrease in SCC of the initial chloride peak. The

low concentration caused a greater decrease in the stimulated Cl$^-$ secretion. There was a

significant decrease in stimulated SCC for the first peaks of the CNT treated cells

compared to the control. NPPB caused a further decrease in Cl$^-$ secretion when it was

added at time = 20 min, indicating that while there was a decrease in chloride secretion in

the cell, the chloride channels were still functional, Fig. 22.

TEER is a measure of barrier function in epithelial cells. This was also calculated

for each tissue to assess the viability of the cells after CNT treatment.
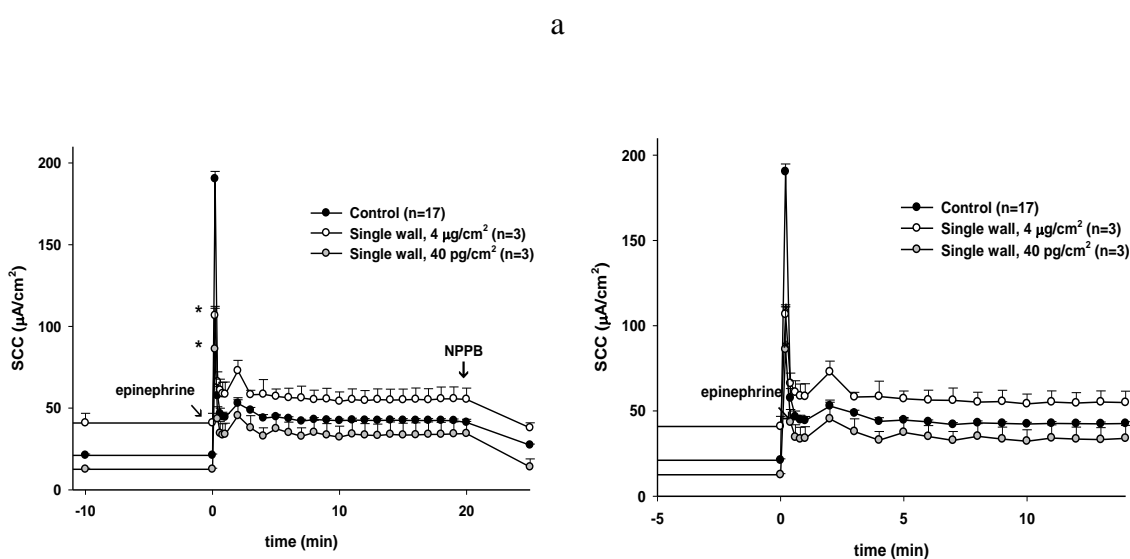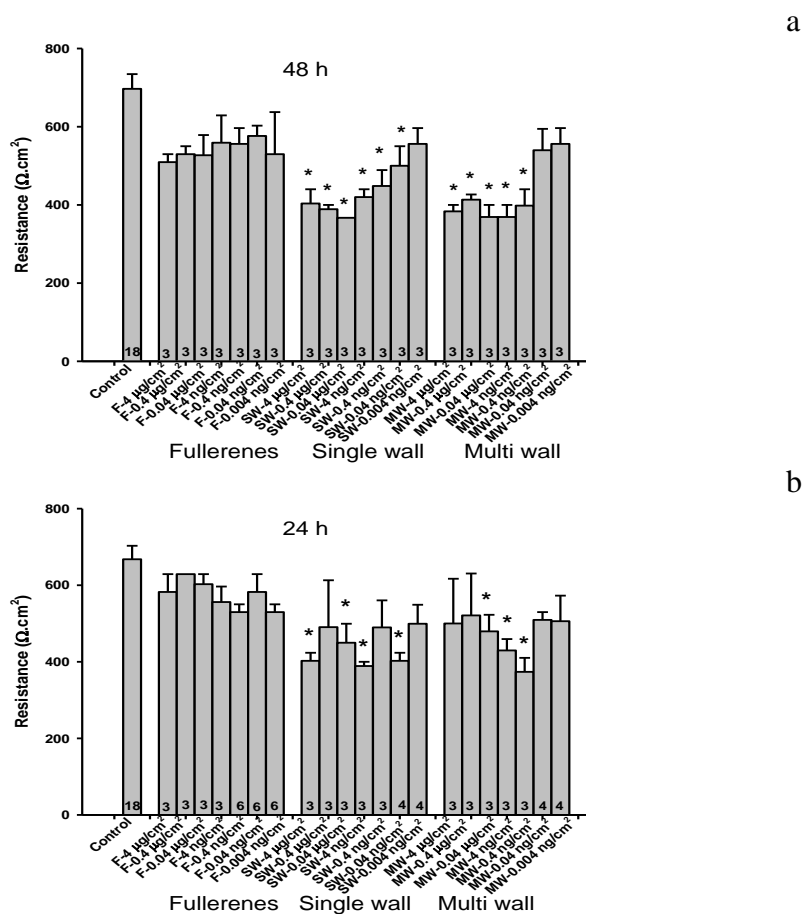

Figure 23: Calu-3 cells were grown to a confluent monolayer on Transwell polycarbonate permeable membranes for 14 days. Effects of incubated fullerenes, SWCNTs and MWCNTs on TEER of Calu-3 cells. (A) Results of 48 h exposures with CNTs. (B) Results of 24 h exposure with CNTs. The numbers in the bars represent the numbers of replicate experiments done for each concentration of CNTs and control. The * above the bars indicate the sample groups which were shown to be statistically significantly different from the control by Students't-test analyses, p<0.05. *Note*. Adapted from: *Cellular Physiology and Biochemistry*, p. 197-212, by Banga, Witzmann, Petrache & Blazer-Yost, (2012).

Calu-3 cells' TEER was significantly decreased due to exposures to select

dosages of SWCNTs and MWCNTs, but it was not changed due to exposures to

fullerenes for both 24 h and 48 h exposure times. Cells exposed to SWCNTs for 48 h showed decreases in TEER due to concentrations ranging from 4 µg/cm^2 to 40 pg/cm^2. Those cells exposed to the MWCNTs, for the same time, had decreases in TEER due to concentrations ranging from 4 µg/cm^2 to 0.04 ng/cm^2. After 24 h incubations, cells had decreases in TEER due to 4 µg/cm^2, 0.04 µg/cm^2, 4 ng/cm^2, and 0.04 ng/cm^2 concentrations of SWCNTs. Cells exposed to MWCNTs, for the same time, had decreases in TEER due to 0.04 µg/cm^2, 4 ng/cm^2 and 0.4 µg/cm^2. These data indicate that there was a greater effect for the doses with the 48 h exposure time, compared to the shorter exposure time, Fig. 23.

3.4 Characterization of T84 cells

Figure 24: T84 cells were grown to a confluent monolayer on Transwell polycarbonate permeable membranes for 14 days. Cell response to secretin stimulation showed an increase in SCC and no significant change when amiloride was added at time = 20 min. The figure on the right shows the stimulation with secretin after pretreatment with amiloride (10^{-5} M) added at time = -10 min.

The T84 cell line is a transplantable human colon carcinoma cell line which was used to simulate the effect of CNTs on the gastrointestinal barrier epithelial tissue, specifically the colon epithelia. T84 cells were grown to confluence, then mounted onto

Ussing chambers and were used for electrophysiological measurements. The cells were stimulated with secretin to measure the cell's response.

In Fig. 24, the graph on the right shows that there was a small decrease in the baseline SCC when the cells were pretreated with amiloride for 10 min. When secretin was added at time = 0 min there was an increase in SCC that was not significantly different from the control peak. The data confirm that the majority of the ion movement was not due to the Na^+ flux via ENaC.

NPPB is a non-specific chloride and potassium channel blocker; it was added to test for the presence of chloride channels in the T84 cell line.

Figure 25: T84 cells were grown to a confluent monolayer on Transwell polycarbonate permeable membranes for 14 days. T84 cells response to secretin stimulation after pretreatment with NPPB at time = -10 min followed by addition of amiloride at time =20 min.

Fig. 25 shows that the addition of NPPB caused a decrease in SCC which lasted for about 5 min and returned to baseline current. NPPB blocked all the chloride channels which were regulating the baseline and the stimulated SCC. There was no further

increase in SCC when secretin was added at time = 0 min and the baseline current

continued to decrease further toward 0 $\mu A/cm^2$. Amiloride added at time = 20 min

showed that the stimulated SCC was not sodium absorption.
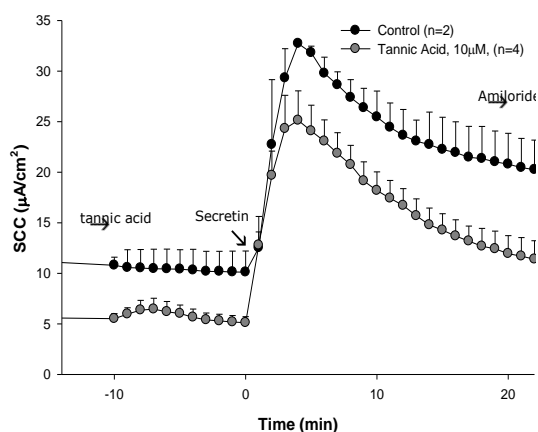
Figure 26: T84 cells were grown to a confluent monolayer on Transwell polycarbonate permeable membranes for 14 days. T84 cells response to secretin stimulation time =0 after pretreatment with tannic acid at time = -10 min followed by addition of amiloride at time =20 min
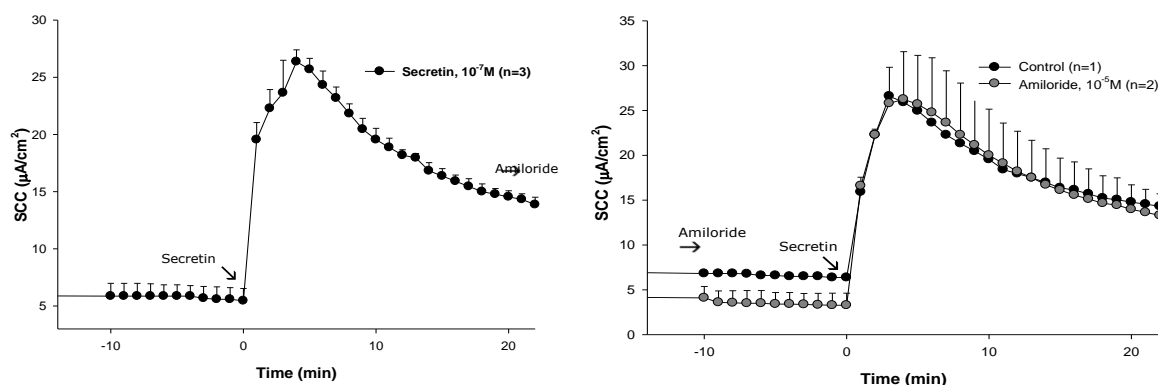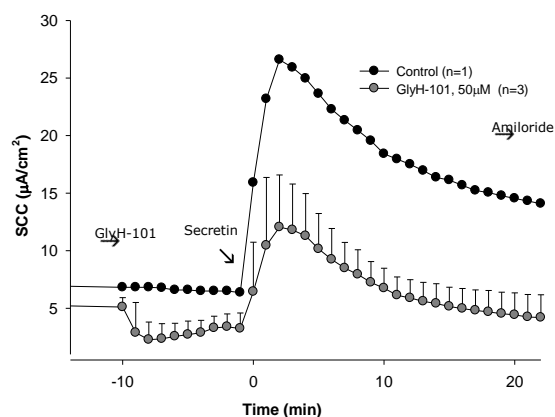
Figure 27: T84 cells were grown to a confluent monolayer on Transwell polycarbonate permeable membranes for 14 days. T84 cells response to secretin stimulation after pretreatment with GlyH-101 at time = -10 min followed by addition of amiloride at time =20 min

Fig. 26 shows that there was no difference between the magnitude of the response

in the cells pretreated with tannic acid, the TMEM16a inhibitor, and the control cells.

These data suggest that there was no TMEM16a in the T84 cell line. Fig. 27 shows

pretreatment with GlyH-101, a CFTR inhibitor. Data show that there was a significant

decrease in baseline current after the inhibitor was added, as well as a partial inhibition of

secretin stimulated SCC. The data indicate that the baseline current as well as stimulated

SCC was predominantly due to the CFTR chloride channel.

The T84 cells were then treated with a specific CFTR inhibitor, CFTR inh-172. When the inhibitor was added at time = -10 min there was a decrease in the baseline current which was sustained for approximately 10 min. Stimulation with secretin at time = 0 min caused a small elevation of the SCC. These results are in agreement with the partial inhibition of secretin-stimulated transport by GLYH-101, Fig. 28.
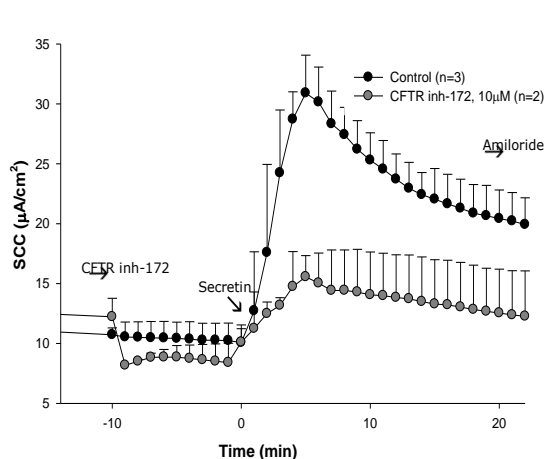
Figure 28: T84 cells were grown to a confluent monolayer on Transwell polycarbonate permeable membranes for 14 days. T84 cells response to secretin stimulation time =0 after pretreatment with CFTR ihn-172 at time = -10min followed by addition of amiloride at time =20 min
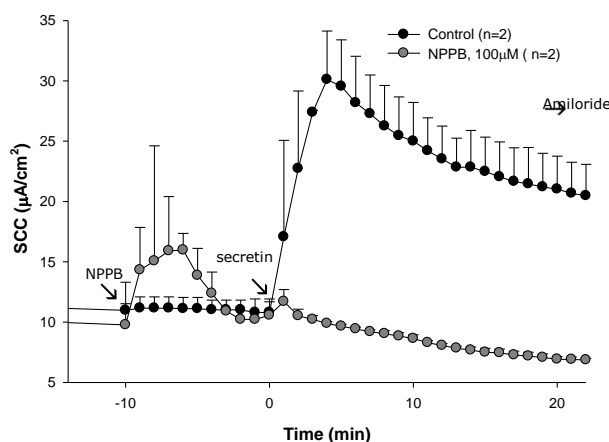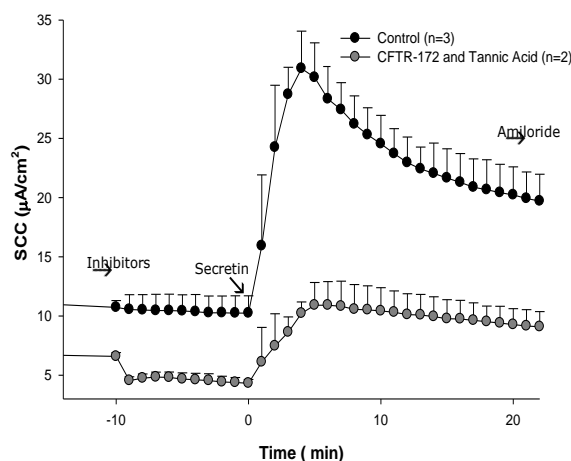
Figure 29: T84 cells were grown to a confluent monolayer on Transwell polycarbonate permeable membranes for 14 days. T84 cells response to secretin stimulation after pretreatment with CFTR-inh 172 coupled with tannic acid at time = -10 min followed by addition of amiloride at time = 20 min

With the pretreatment of the T84 cells with CFTR inh-172 and tannic acid, there was a decrease in baseline current for the duration of the pretreatment period. When secretin was added at time = 0, there was a partial inhibition of the stimulated transport that was similar to that of the CFTR inhibitor alone. The data showed that the baseline and stimulated SCC in T84 cells can be elevated by the cAMP increasing agent secretin and is largely due to the action of CFTR, Fig. 29.

The T84 cell line was treated with doses of raw, pristine and acid treated pristine short MWCNTs to simulate the effect of these nanotubes on the digestive tract.

3.5   Dose response on T84 cells
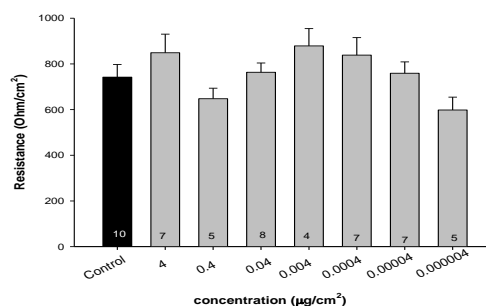
Figure 30: Effect of raw short MWCNTs on TEER in cells incubated for 48 h. The number of replicate experiments for each concentration is indicated as the values in the bars. T84 cells were grown to a confluent monolayer on Transwell polycarbonate permeable membranes for 14 days.
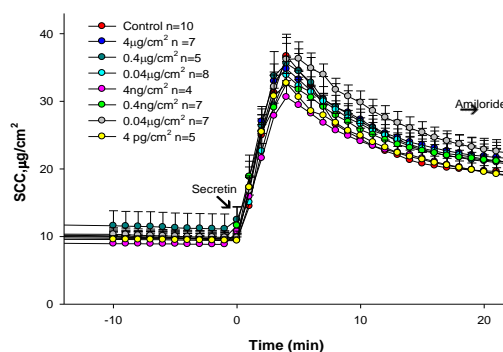
Figure 31: Effect of raw short MWCNTs on secretin stimulated SCC in cells incubated for a 48 h. Amiloride added at time = 20 min had a slight decrease in SCC indicating the presence of a small amount of ENaC. T84cells were grown to a confluent monolayer on Transwell polycarbonate permeable membranes for 14 days. Students' t-test showed that there was not a statistically significant difference between the mean peak values of the control and the raw short MWCNTs treated T84 cells.

Raw short MWCNTs were incubated with the cell line for 48 h to simulate the maximum time it may take for the CNTs to remain in the digestive system before being

cleared. Treatment with these raw short MWCNTs had no statistically significant effect

on the TEER or baseline and stimulated SCC of the T84 cells, Figs. 30 and 31. These

cells secreted mucus onto their surface while the cells were becoming confluent. These

secretions may serve to protect the cell line from the topical CNT applications. Further

treatment was done on the T84 cell line using pristine short MWCNTs.
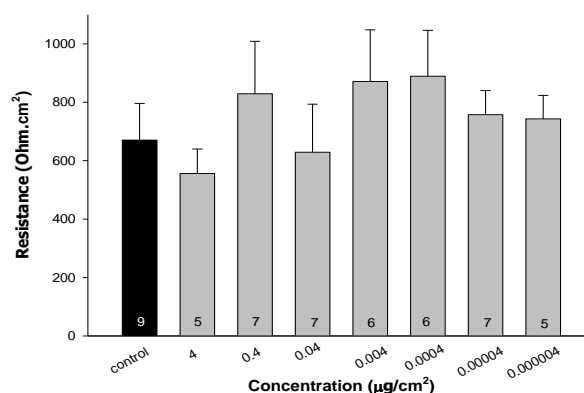
Figure 32: Effect of pristine short MWCNTs on TEER in T84 cells incubated for a 48 h time point. The number of replicate experiments for each concentration is indicated as the values in the bars. Cells were grown to a confluent monolayer on Transwell polycarbonate permeable membranes for 14 days. Students' t-test showed that there was not a statistically significant difference between the mean values of the control and the pristine MWCNTs treated T84 cells.
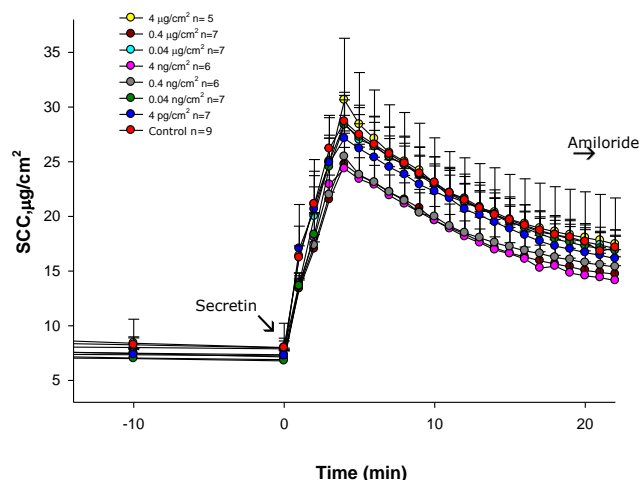
Figure 33: Effect of pristine short MWCNT on secretin stimulated SCC in cells incubated for a 48 h time point. T84cells were grown to a confluent monolayer on Transwell polycarbonate permeable membranes for 14 days. Amiloride added at time = 20 min had a slight decrease in SCC indicating the presence of a small amount of ENaC. T-test comparison showed that there was not a statistically significant difference between the mean values of the control and the pristine short MWCNTs treated T84 cells.

There was no difference in the stimulated SCC or TEER for the pristine short MWCNTs treated cells and the control. T84 cells form high resistance tight junctional complexes, of up to 1100 Ω.cm^2, when they become confluent.

In order to assess whether the fluids of the GI tract may influence the activity of the CNTs, we acid treated, then neutralized the CNTs with simulated gastric fluid and simulated intestinal fluid respectively. Treated CNTs were then added to cell culture media and incubated with the cells for 48h. The TEER and secretin stimulated SCC were measured for all concentrations in log dose units from 4μg/cm^2 to 4pg/cm^2, except 0.4 and 0.0004μg/cm^2.
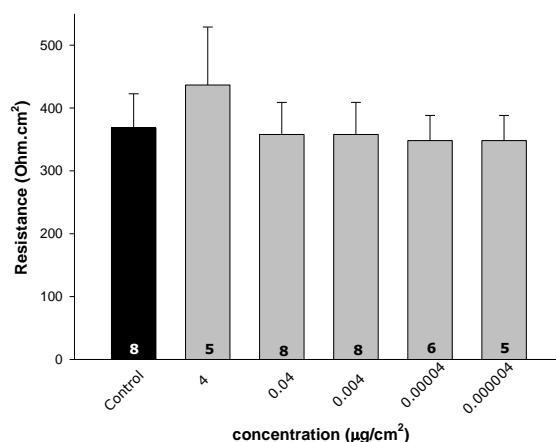
Figure 34: Effect of acid treated short MWCNTs on secretin stimulated SCC in cells incubated for a 48 h time point.T84cells were grown to a confluent monolayer on Transwell polycarbonate permeable membranes for 14 days Amiloride added at time = 20 min had a slight decrease in SCC indicating the presence of a small amount of ENaC. Students't-test comparison showed that there was not a statistically significant difference between the mean values of the control and the acid-treated pristine short MWCNTs treated T84 cells.
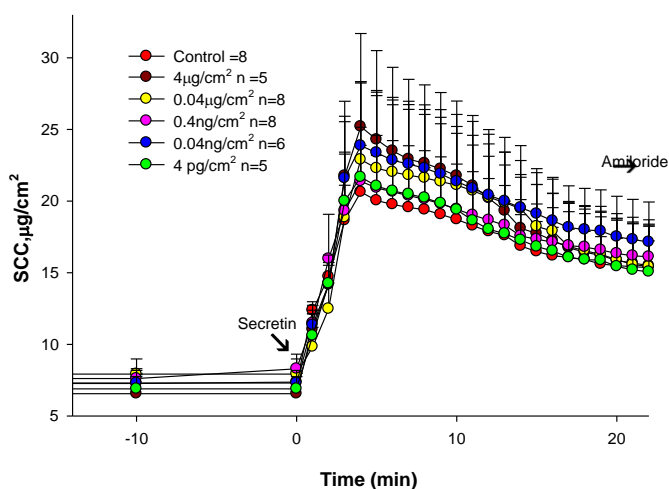
Figure 35: Effect of acid treated short MWCNTs on secretin stimulated SCC in cells incubated for a 48 h time point. T84cells were grown to a confluent monolayer on Transwell polycarbonate permeable membranes for 14 days. Amiloride added at time = 20 min had a slight decrease in SCC indicating the presence of a small amount of ENaC. T-test comparison showed that there was not a statistically significant difference between the mean values of the control and the acid treated prisine short MWCNTs treated T84 cells.

Overall, the data in Figs. 30 to 35 show that there was no statistically significant effect of the short MWCNTs on the TEER or stimulated SCC of the T84 cell line.

To determine whether the CNTs had induced any inflammatory responses in the cell monolayers, we conducted cytokine assays on them. We used the Quantikine ELISA human TNF-α and human CXCL8/IL-8 Immunoassay kits, to test for the presence of TNF-α and IL-8 respectively. Cytokines are extracellular signaling proteins produced by one cell to act on others in order to modulate intracellular functions or recruit other cells to a site of injury. The data for TNF- α and IL-8 reflect the intensity of color developed in proportion to the amount of cytokine that was bound in the initial step of the assay.

IL-8 is a member of the CXC chemokine receptor family. A wide variety of cells secrete IL-8 when they are exposed to inflammatory stimuli, and these include monocytes and neutrophils, fibroblasts and keratinocytes, mast cells, visceral and smooth cells, dendritic cells, type 1 greater alveolar cells and endothelial cells. The T84 cell line has been shown to also secrete IL-8 in response to exposures to the bacterial V. cholera flagellin (Harrison et al., 2008). There are two G-protein- coupled receptors for IL-8; these are CXCR1, which responds to low IL-8 concentration and CXCR2, which responds to high IL-8 concentration, which share 77% amino acid (aa) identity. These proteins are known to homodimerize and may also heterodimerize but will disassemble following IL-8 binding.

3.6   Cytokine assay

3.6.1   IL-8 assay

b
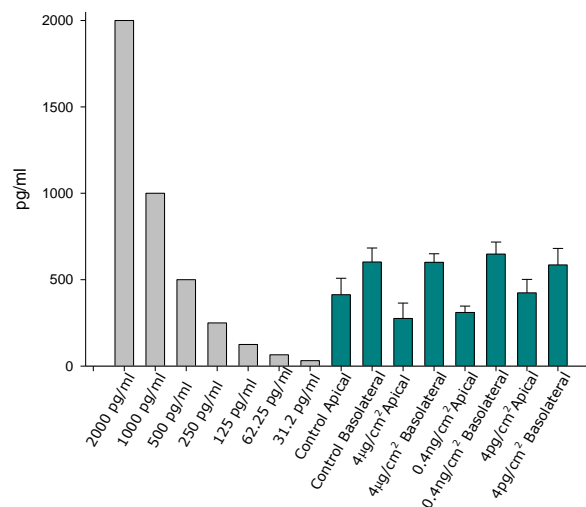
Figure 36: Release of cytokines due to exposures to pristine short MWCNTs for 48 h. Confluent T84 cells were exposed to concentrations 4µg, 4ng and 4pg/cm^2. Apical and basolateral media were extracted from the transwells and used for the assay.

Table 3: Release of cytokines fom T84 cell monolayers due to exposures to CNTs. Confluent T84 cells were exposed to 4µg, 4ng and 4pg/cm^2 pristine short MWCNTs for 48 h. Apical and basolateral media were extracted from the transwells and used for the assay. BR indicates the OD readings that were below range of the standard curve. The values indicate the cytokine levels from the basolateral and apical media compartments in pg/ml.

Control		4µg/cm^2		4ng/cm^2		4pg/cm^2	
Apical	*Basolateral*	*Apical*	*Basolateral*	*Apical*	*Basolateral*	*Apical*	*Basolateral*
BR	*BR*	*BR*	*BR*	*BR*	*BR*	*BR*	*BR*
473.2	718.1	BR	640.3	307.4	530.6	BR	530.6
538.7	446.4	364.9	659.1	375	771.6	501.4	771.6
227.84	642.1	186.2	502.8	248.2	642.1	345.8	454.6

The data values for the samples and the standards show the corrected final concentrations. The original reported OD values (from the spectrophotometer) were averaged and the average blank values were subtracted from the sample and standard averages. Fig. 36 shows the levels of IL-8 which was measured in the standards and samples in pg/ml. The control IL-8 concentration ranged from 642.1-718.1 pg/ml on the standard curve, but these values were not reflective of an inflammatory response, Table 3. The levels of IL-8 in the control samples were not different from the levels found in the experimental samples. A Student's t-test's report showed that there was no statistical difference between the IL-8 levels in the apical control media compared to the experimental samples; there was also no significant difference between the basolateral control IL-concentration and that of the basolateral experimental samples.

Fig. 36 also shows that basolateral IL-8 levels were greater than the apical IL-8 levels. In a study done by Eckmann, Kagnoff, and Fierer (1993), in which polarized T84 cells were infected with S. Dublin, L. monocytogenes, and S. dysenteriae, there was a total of 80% of the secreted IL-8 concentration measured in the basolateral compartment. These findings showed that the monolayer preferentially secreted the IL-8 at the basolateral surface. This previous data may explain why the levels of IL-8 were higher in the basolateral media samples compared to the apical media samples.

The Quantikine ELISA Human TNF-α Immunoassay was used to measure human TNF-α in the cell culture supernates of confluent T84 monolayers that had been exposed to various concentrations of pristine short MWCNTs for 48 h. The data reflected the intensity of color developed in proportion to the amount of TNF-α bound in the initial step. TNF-α, also known as cachectin, is the prototypic ligand of the TNF

superfamily. This molecule is important because of its role in inflammation, immune system development, lipid metabolism and apoptosis. It is secreted by immune, epithelial, endothelial cells and tumor cells.

The TNF-α OD values were below the standard curve range values. The assay kit instructions recommended a 100 fold dilution, yet even after decreasing the dilution factor to 10 or 2 the OD values reported were below the range of the standard curve.

While the CNTs had no significant effect on the T84 cell line cytokine release, there were significant changes in TEER and stimulated SCC in the Calu-3 cell line. Changes in this epithelial cell line indicated that the CNTs may be affecting barrier epithelia; hence, this prompted us to investigate how these CNTs were interacting with the cells after they were applied on top of the monolayer of cells. We first investigated their effect on the cells' first line of defense, the plasma membrane, by using model Bilayer lipid membranes (BLM).

3.7   CNTs on bilayer lipid membranes

3.7.1   CNTs on bilayer lipid membranes only

Plasma membranes are composed of bilayers of neutral and electrically charged lipids (Hall & Baker, 1977). The synthetic lipid membranes used in this study were formed from neutral phosphatidylcholine (PC) and negatively charged phosphatidylserine (PS) lipids. Membranes were formed using a Planar Bilayer Workstation (Black Lipid Membrane) from Warner Instruments. The protocol for membrane formation, data acquisition and analysis are detailed in sections 2.14 and 2.15. With this instrument, we monitored ionic currents when a voltage was applied across the bilayer lipid membrane.

Once the membrane was synthesized there was a characteristic flat baseline which remained at the 0 pA level even when a voltage of up to 300 mV was applied. However, when the GA protein was added, a characteristic current was able to be measured as a function of applied voltage. Oiki, Koeppe and Andersen (1995) explained that GA channels are formed by the dimerization of a pair of nonconducting monomers within the membrane and they further explained that the channel closing is as a result of the dissociation of the dimer within the membrane.
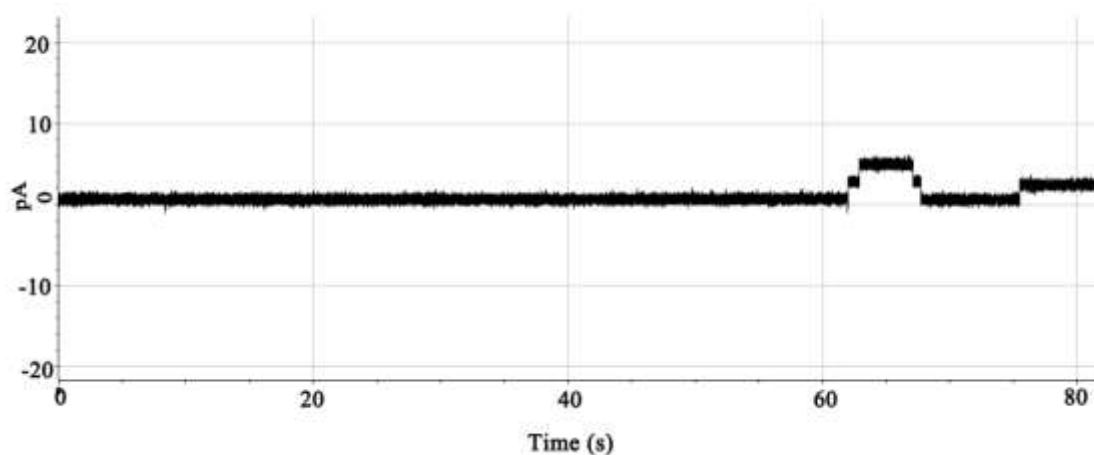
Figure 37: A representative recording of current as a function of time with the DPhPC lipid at 100 mV. 0.5 μl of 10^{-13} M GA was added to the membrane at time = 0 min.

Fig. 37 shows a typical ion-channel recording as a function of time. For the period of 0 to 62 s, the plot shows a flat baseline, indicative of an intact lipid bilayer followed by steps of current due to the opening of GA channels. Lipid membranes are impermeable to ions without the presence of proteins or peptides which facilitate water or ion movement across the cell (Langecker et al., 2002). At time = 62s, there was an increase in current, which is representative of a single open channel in the membrane. The second increase in

current, time = 63 s, was followed by a steady current (flat line) which represented the duration of time the two channels remained open, ~ 4s. The decrease in current at time = 67s and 68s indicated the sequential closing of the two channels and the signal returned to baseline.

GA is either in monomer or in dimer form, with the dimer constituting a membrane-spanning channel. The channels form from two right-handed, single-stranded β-helical monomers with 6.3 residues per turn that form a head to head dimer. It allows positive monovalent ions to pass through it, generating an ionic current when a voltage is applied across the membrane (Rostovtseva, Petrache, Kazemi, Hassanzadeh, & Bezrukov, 2008; Grisham et al., 1997).

The effect of CNTs on the membrane without GA was measured in the presence of 0.8 ng/ml and 80 ng/ml of short raw CNTs or serum free media, which was the control, to the KCl buffer system. CNTs were prepared in the same method as described in section 2.1 but the autoclaved CNT-FBS mixture was dissolved in serum free media instead of FBS-supplemented cell culture media. Initial experiments with the FBS containing media proved difficult because of the large protein content in the media.

The data in Fig. 38 shows a representative part of the whole trace where the effect of the CNTs on the membrane was detected. The first part of the trace, time 0 to122s, showed no effect of CNTs on the baseline. The deflections after time = 130s show the current increasing at irregular intervals. These transient deflections induced by the presence of CNTs show that the nanotubes may cause spontaneous ion movement across the membrane. In Fig. 39 the addition of the low concentration of CNTs was less effective and showed fewer and shallower deflections of the membrane.
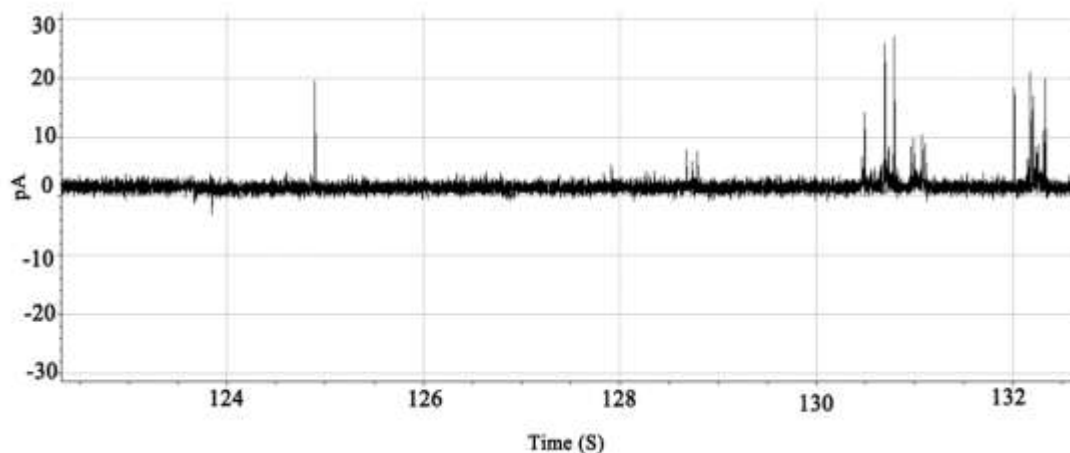
Figure 38: Regions of the trace which showed the most effect of 0.80 μg/ml short MWCNTs. Synthetic lipid membranes were formed in a small hole within the teflon tape separating the wells in the bilayer chamber. Membranes were formed with the neutral lipid-DPhPC in the KCl buffer solution. A voltage of 50 mV was added to the membrane.
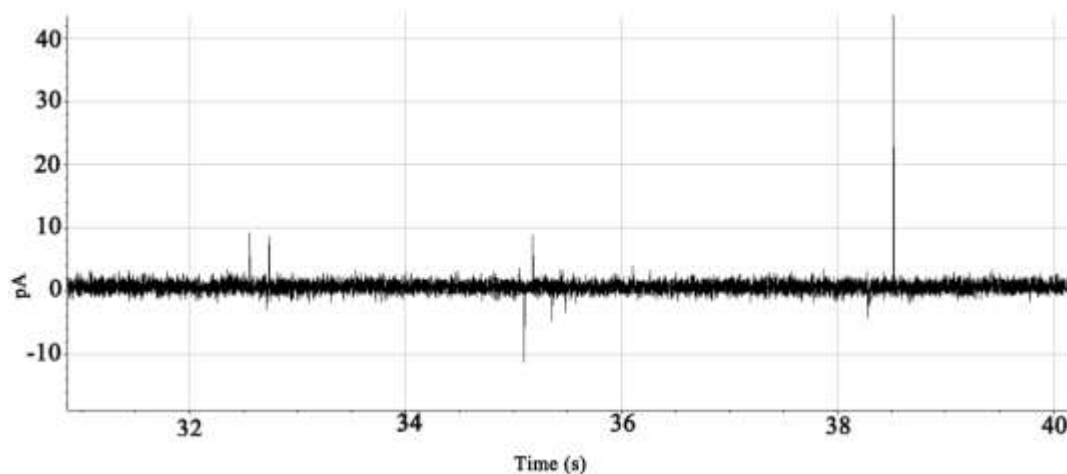
Figure 39: Regions of the trace which showed the most effect of 0.80 ng/ml short MWCNTs. Synthetic lipid membranes were formed in a small hole within the teflon tape separating the wells in the bilayer chamber. Membranes were formed with the neutral lipid-DPhPC in the KCl buffer solution. A voltage of 50 mV was added to the membrane.

The pure lipid bilayer was treated with various concentrations of CNTs. The first 300s of the trace was analyzed after the first sign of activity was noted. The changes in baseline slope and deflections of the trace in the presence of CNTs were analyzed using

the Clampfit software. This analysis software calculated the maximum rise in slope for the entire time the membrane remained exposed to the nanotubes and averaged these values against the control (baseline). Fig. 40 shows that there was a no difference in maximum rise slope in the CNT treated membranes compared to the untreated membranes. Although the values appeared to be different, a Students' t-test showed that there was no significant difference between the CNT treated membranes and the control for both the short, $p= 0.184$, and long MWCNT, $p=0.292$.
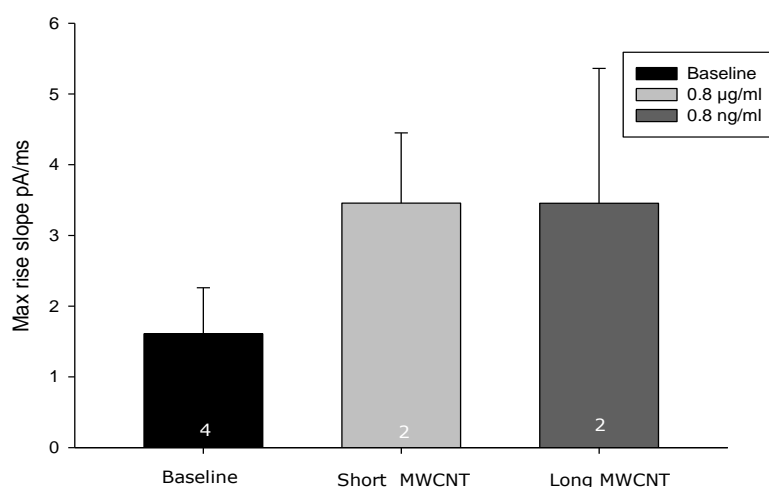
Figure 40: Histogram illustrating the differences in the maximum rise slope, pA/ms, of traces that were untreated and treated with short and long MWCNTs.

3.7.2   The effect of CNTs on GA activity in bilayer lipid membrane

Plasma membranes are composed of both lipids and proteins; therefore, we sought to investigate the effect of CNTs on an ion channel reporter protein's activity, GA. GA was added to the lipids followed by doses of CNTs and the channel number and open channel probability was calculated using theoretical binomial distribution plots which

were generated numerically (using Perl software). The amount of current generated by a single open GA channel was ~2pA, and this value was used to determine the number of channels open at the same time. One important parameter for the analysis of ion channels is the probability value (p) that the channel is open at some moment in time. For a channel that stays mainly open, p is a number between 0.5 and 1, while for a channel that stays mainly closed, p is between 0 and 0.5. The probability to have n channels open at the same time depends on this p value and also depends on the total number N of channels present in the membrane during the measurement. If the N channels are equivalent and independent, the probability of having n channels open at the same time is given by a particular distribution function (binomial) with the formula below, which was used to calculate the theoretical graphs using the following equation, $f(n) =$

$$\frac{N!}{n!(N-n)!}\, p^n(1-p)^{N-n}.$$

DPhPC was a more stable lipid and allowed GA to form more single channels in the membrane, hence having higher relative abundances of peaks at lower amplitudes (far left) as depicted in the graph. This was followed by a characteristic decrease in relative abundance of higher channel numbers, as seen in Fig. 41.

3.7.3   Control, GA with bilayer lipid membrane
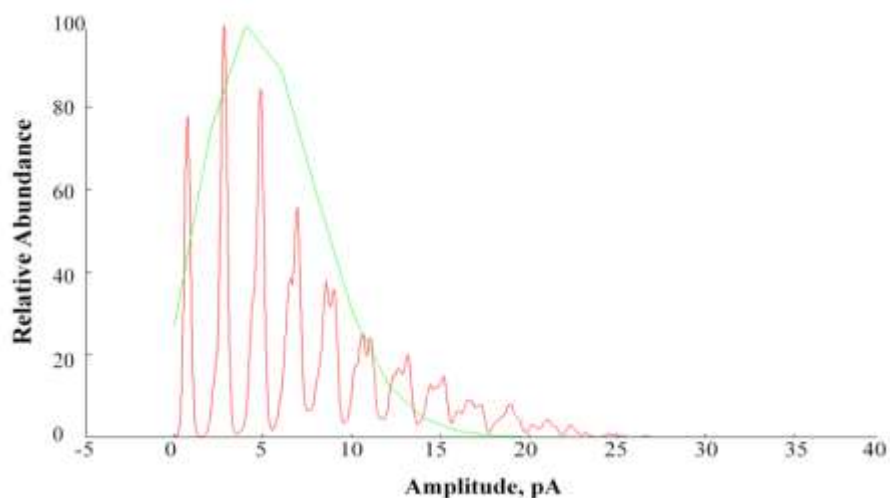
Figure 41: Graph showing the channel probability in DPhPC which was determined by matching histograms (red) with precalculated binomial distribution plots. Lipid membranes were formed and 1μl of 10^{-13} M GA was added. After treating the membrane with the gA protein the channels were recorded for 1- 1.5 h. (green) .

DPhPS is a negatively charged lipid which showed much more channel activity

with GA than the neutral lipid. There may have been electrostatic interactions between

the channel protein and lipids responsible for this behavior. There were multiple channels

open at a single time and fewer single channels overall, Fig. 41. Compared to the PC

representative graph, there were only 170 channels in the PS lipid, which has an open

channel probability of 0.0275; whereas, there were 80 channels open with the PC lipid

and an open channel probability of 0.033. These trends show that the neutral lipid allows

more stable channel formations to occur.
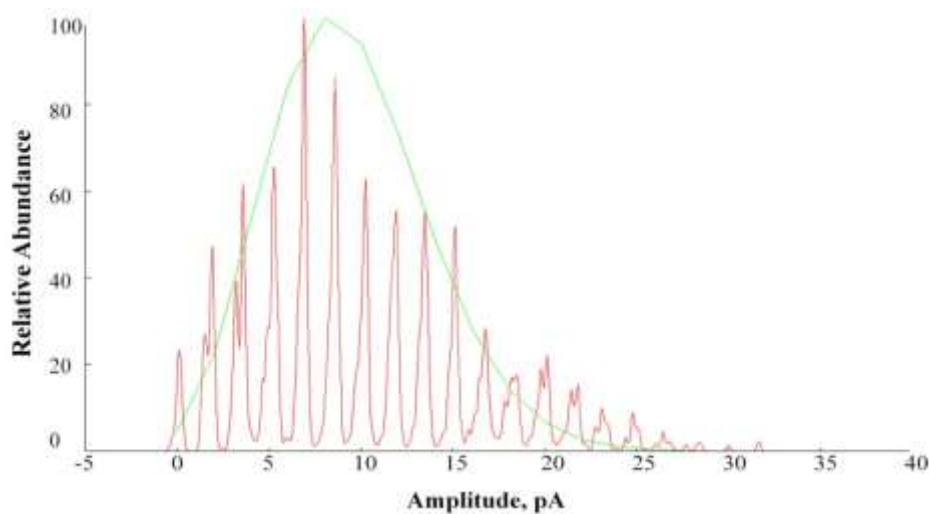
Figure 42: Graph showing the channel probability in DPhPS which was determined by matching histograms (red) with precalculated binomial distribution plots. Lipid membranes were formed and 1µl of 10^{-13} M gA was added. After treating the membrane with GA the channels were allowed to propagate for 1- 1.5 h. distributions (green)

Serum free media was the control for the nanotube-GA experiment. SF media was added to the KCl buffer and the effect of the media was observed on the channel activity. There was an increase in multiple open channels in the membrane with the media present. The graph resembled the channel activity of the negatively charged lipid more than DPhPC.

3.7.4 Serum free media on GA in bilayer lipid membrane
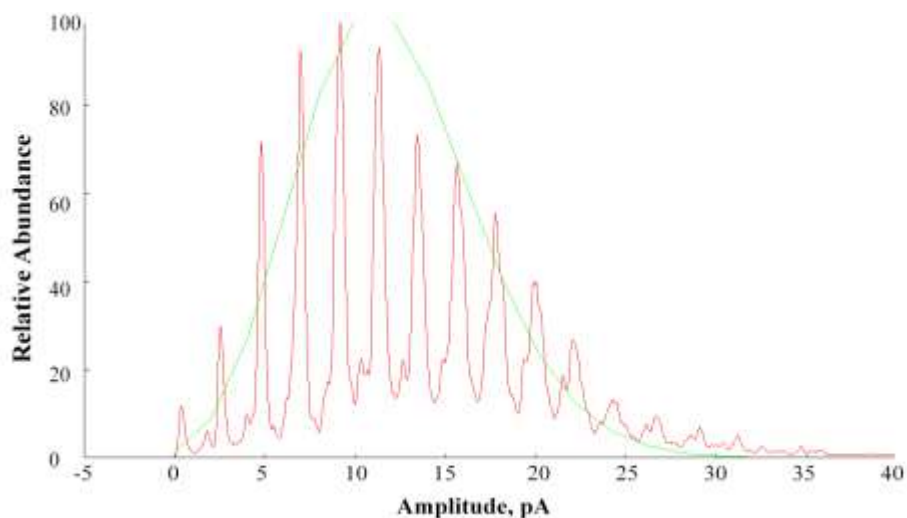
Figure 43: Graph showing the channel probability in DPhPC which was determined by matching histograms (red) with precalculated binomial distribution plots. Lipid membranes were formed in DPhPC and 1μl of 10^{-13} M GA was added. Serum free media was then added to the membrane. After treating the membrane with GA the channels were allowed to propagate for 1- 1.5 h.

Further assessment was done with the CNT dosages on the GA activity in the membrane of the PC and PS lipids. The data for the effect of CNTs on the GA activity in the PS lipid are not shown because the membrane broke when the CNTs were added to the buffer system. This reaction may be relevant to determine the toxicity of the CNTs on the cells. On the other hand, nanotubes added to the PC membrane caused an increase in the number of single channels in the membrane compared to the control.

3.7.5   Low concentration CNTs on GA in bilayer lipid membrane
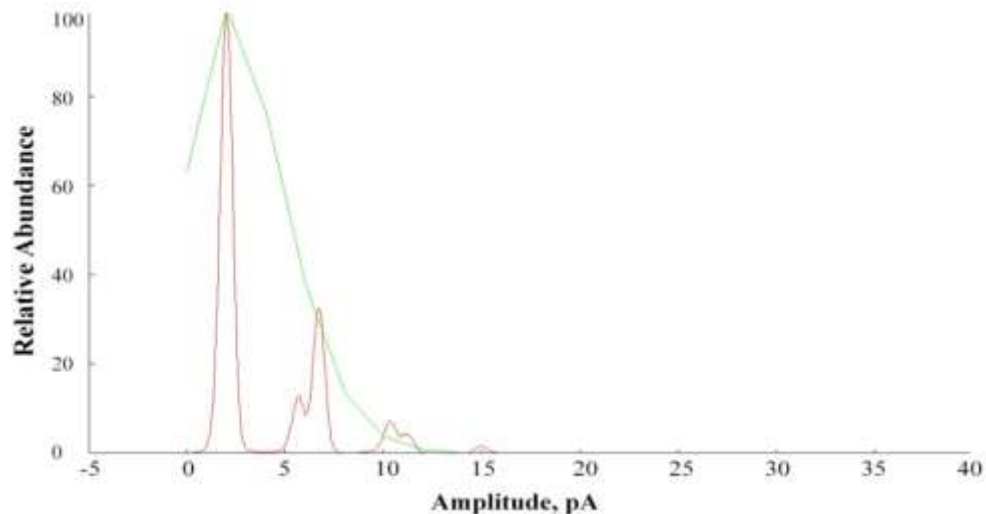
Figure 44: Graph showing the channel probability in DPhPC which was determined by matching histograms (red) with precalculated binomial distribution plots. Lipid membranes were formed using DPhPC and 1μl of 10^{-13} M GA was added followed by 0.8 ng/ml short

Figure 44 shows the large number of single channels which resulted when the nanotubes were added to the neutral lipid with GA. The theoretical graph which matched this plot indicated that there was a maximum of 30 channels opened in the membrane at a single time and the probability of these open channels was 0.05. Many other data graphs were not able to be assessed using the generated theoretical graphs because the membranes broke when the CNTs were added in the presence of the GA.

Figure 45 shows the effect of the nanotubes after 20 min of CNT-GA interactions in the membrane. After 21 min of the recording, the membrane broke. It was noted that while the open channels were not clearly defined, there was an increase in current as depicted by the markers. At marker 2 the current had increased from baseline to 7.08 pA and to 19.74 pA at marker 3.
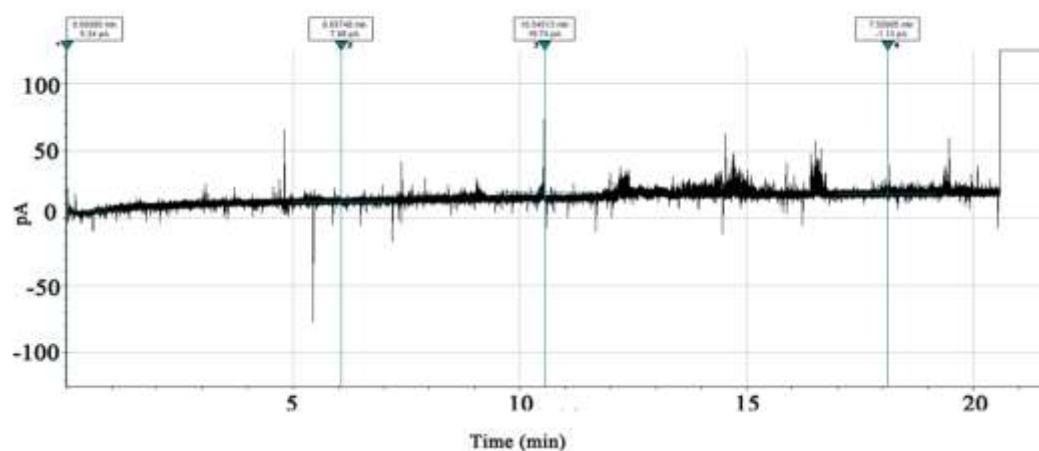
Figure 45: Effect of 80 ng/ml short MWCNT on the lipid membrane. Lipid membranes were formed using DPhPC and 1μl of 10^{-13} M GA was added followed by the CNTs. The membrane broke at time = 21 min.

In Fig. 46 there was another effect on the GA channel's activity. The open channels were not defined and there was an increase in channel activity with additional large deflections in the trace, similar to those seen in Figs. 38 and 39, when the membrane was treated with the nanotubes only. Further, it was noted that the membrane remained intact while the membrane currents rose to 313 pA and continued to increase even after 1 hr.
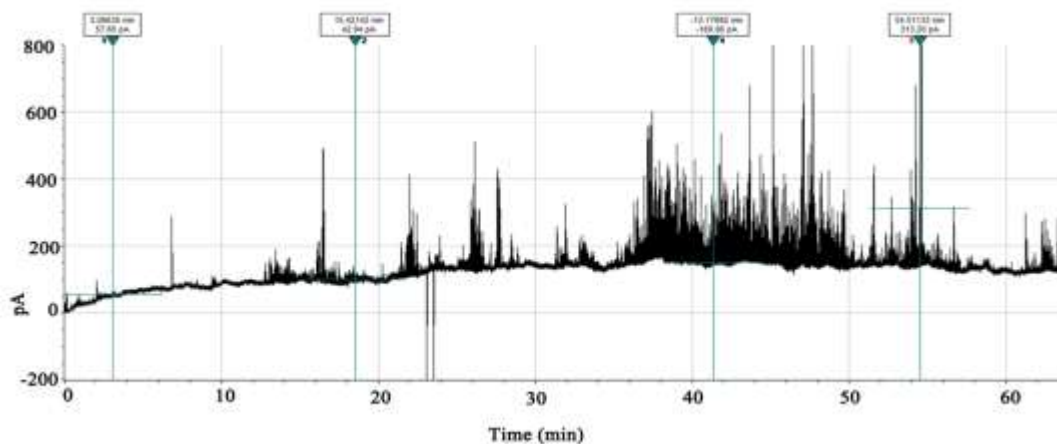
Figure 46: Effect of 0.8 ng/ml short MWCNT on the lipid membrane. Lipid membranes were formed using DPhPC and 1μl of 10^{-13} M GA was added. The individual channels were not defined but the membrane currents increased to over 200pA.

The lipid combination, maximum number of channels, and open probability data

was summarized in order to show the general effect of the CNTs activity on the

membrane. The data was determined by matching the resultant trace's histograms with

precalculated binomial distributions which were generated using eqation 1.

Table 4: The channel number and probability of an open GA channel was determined by matching the data set with pre-calculated theoretical binomial distributions.

Lipid with GA	Channel number	Probability
DPhPC	10	0.01
	80	0.0125
	80	0.033
	160	0.06
DPhPS	35	0.055

Table 4 continued

	Channel number	Probability
	170	0.0275
	170	0.07
Lipid with GA	**Channel number**	**Probability**
DPhPC and SF Media	45	0.075
	100	0.06
	170	0.035
DPhPC, GA and 0.8 pg/ml	3	0.05
DPhPS, GA and CNTs	Data is not shown because membrane broke when CNTs when added.	

There were higher numbers of single channels and smaller numbers of multiple channels generated in the DPhPC membrane compared to the DPhPS membrane. This could be attributed to the difference in lipid charge. The nanotubes were interfering with the channel number as well as the definition of the channels. While some of the data was difficult to analyze it was generally seen that the barrier function of the membrane was reduced as the current levels rose in the presence of the CNTs, and in some cases the membranes broke.

CHAPTER 4. DISCUSSION

Many studies are being conducted to investigate the toxic effects of CNTs on human biological systems. There are numerous studies which show that CNTs, including raw and functionalized, are toxic to epithelial cells. In one particular study Poland et al., (2008) showed that unfunctionalized MWCNT may pose a carcinogenic effect in treated mice. In this particular study several female mice were injected intraperitoneal (i.p) with 50 μg of nanotube samples and then the subjects were sacrificed on day 7. TEM images of the lung tissue showed granulotamous inflammation in the peritoneal lining. Granulomas form from an accumulation of macrophages. These immune cells are recruited to a site of infection in order to eliminate the foreign material. In another study Hirano, Kanno and Furuyama (2008) used the mouse macrophage cell lines, J774.1 and CHO-K1, which were cultured on cover slips with 20 μg/mL MWCNTs for 4 h or 8 h. SEM images of the exposed cells showed pseudopodial extensions of the macrophage's plasma membrane extending along the length of the MWCNTs. Some images showed macrophages that were punctured by nanotubes because the nanotubes might have been too large to engulf. These findings indicate that this may cause an overall decrease in particle clearance activity at the site of nanotube exposure due to injury sustained by the macrophages. These studies are representative of many other findings which indicate that raw nanotubes are potentially toxic to humans since they are difficult to eliminate. In a

more recent study, Zhang et al. (2012) showed that when the alveolar tissue of mice

exposed to functionalized-SWCNTs were examined there were many residues 14 days

after exposure. These data suggested that the nanotubes had the potential to persist in the

lungs for extended periods of time. This prolonged exposure was also suggested to cause

further cytotoxic effects. Liu et al., (2009) showed that many findings of this nature have

shaken the public's confidence in the use of CNTs for biomedical applications.

Nanotechnology has the potential to change medicine. There are many novel applications

for CNTs, yet there still needs further evidence explaining how these raw CNTs may

interact with the human body via epithelial tissue, thus rendering them potentially toxic.

In this research we sought to explain how these nanotubes may be interacting with

epithelial cell membranes in order to confirm or disprove the risk. These findings may

serve as a platform for manufacturers and consumers to be able to make informed

decisions about their products and applications.

In this study we used raw and purified, short and long, MW and SW CNTs to

determine their effect on the barrier function of epithelial cells and more specifically the

cell membrane. In previous studies done in our laboratory, CNTs were exposed to the

MPK epithelial cell line. These exposures showed significant decreases in TEER and

stimulated SCC (Blazer-Yost et al., 2011). These findings showed that NP exposure

caused decreased in barrier function as well as compromised hormonal response in the

cells.

We sought to investigate the effect of CNTs on the barrier function in the Calu-3

and T84 cell lines in order to simulate their effect on the lungs and digestive system.

These cell lines are derivatives of human airway epithelial tissue and colon epithelial

tissue, respectively. Krug and Wick (2009) explained that inhalation and ingestion are the most prevalent modes by which CNTs enter the body. Inhaled nanotubes will eventually agglomerate on the lung epithelial tissue if they are not first removed by the MCM. Swallowed CNTs may enter the digestive tract and could reach the digestive lining as well. There is great potential for these nanotubes to reach our epithelia; hence, electrophysiology analysis was done to measure their effect on barrier and hormonal function. NPs were first characterized to assess whether they are more likely to interact when in solution or on a surface.

In order to determine the agglomeration potential of the CNTs, we measured their surface charge by zeta potential. NPs potential to aggregate can be measured at the slipping plane. This is the point of intersection between the tightly bound counterions on the surface of the particle and the ions in the solvent phase (Szymczyk et al., 1998). Zeta potential values indicate the stability of a colloid system. Particles which have zeta potential values that are outside the range of -30mV and +30mV are considered to be stable, thus they are able to overcome electrostatic attractions and remain in solution. In contrast, particles that are within the range of -30mV and +30 mV will likely form aggregates when they are drawn to each other due to their low surface charges, and will then function as single larger units. In Tables 1 and 2 the zeta potential values for the CNTs were all within the -30mV and +30mV range. This indicated that the nanotubes have the potential to form aggregates even at these low, physiologically relevant concentrations. Many studies show that the use of high NP concentrations is not physiologically relevant to simulating this effect. Blazer-Yost et al. (2011) showed that in concentrations above 1µg/ml of both SW and MW CNTs, there is significant

agglomeration. Therefore, large nanotube masses may pose a micro effect on the epithelial tissue. In order to adequately assess the nano effect on the tissue we used lower, more physiologically relevant, concentrations. These concentrations ranged from $4\mu g/cm^2$ (100 μg/ml) to $4pg/cm^2$ (100 pg/ml).

Fig. 3 shows short MWCNTs which were prepared in FBS free media. The manufacturer reported dimensions for these tubes were, 1-5 μm long and 46-60 nm in diameter. In Fig. 3a the diameter for the tubes ranged between 4.01 nm to 28.6 nm. These values fall below the manufacturer's measurements and may be due to fragmentation which might have occurred during sonication. Sonication is an important step in the preparation of the nanotube samples. After the nanotubes were serially diluted they were sonicated for 20 pulses using a Branson sonifier. This allowed for even dispersal of the tubes throughout the container; however, these sonications may be the cause of the fragments.   Liu et al. (1998) showed that after mixing long, entangled SWCNTs in a mixture of sulfuric acid, nitric acid and surfactants, short nanotubes appeared to behave like individual macromolecules. In Fig. 5, fragmented nanotubes aligned themselves in bundles which linked to form chains. The long SW nanotube fragments formed bundles with diameters of just under 100nm; however, the manufacturer reported dimensions for the long SW nanotubes were 5-15 μm long and under 2nm in diameter. The data showed that even at low concentrations the nanotubes clumped together. New findings in biomedical research show products developed from complexes of proteins and nanotubes. In one particular study SWCNTs were functionalized and allowed to form complexes with proteins so that they may be taken up by cells for intracellular drug delivery (Kam &

Dai, 2005). While this technique has great promise for medical discovery, the mechanism for the degradation of these materials, after they have delivered their cargo, is lacking.

Figs. 4 and 6 show the TEM images of nanotubes that were made in cell culture media containing serum proteins. The proteins apparently formed compounds with the nanotubes. The zeta potential values for the nanotubes and the control (serum proteins) were all approximately 8 mV. The similarity in surface charge indicated that the proteins may have coated the nanotubes and therefore defined the complex's surface charge. Kam and Dai (2005) explained that a protein-nanotube complex may be formed by NPs encapsulating proteins or by proteins being adsorbed unto nanotubes. The latter interaction was confirmed by our TEM images. In Figs. 4a, 4b, 6a and 6b, we see that there are elongated and globular structures forming long chains of the globules. We assume that they are connected since they are all adsorbed onto the nanotube strands. Lui et al. (2013) explained that when NPs enter the biological environment, proteins adsorb onto their surface to form complexes called protein coronas. These complexes are as a result of hydrogen bonds, van der waal forces, electrostatic forces, Lewis acid forces or entropic effects. These interactions influence the stability of the bond; determining whether it is reversible or irreversible.

Given that NPs undergo surface modification when they enter biological environments, this makes them very versatile. In a study by Kam and Dai (2005), when the SW nanotubes were deliberately conjugated with proteins, they were easily endocytosed by HeLa and NIH-3T3 cell lines because of the familiar protein coating. Therefore, the comlpex which is formed from the nanotubes and proteins serves as a mask for the nanotubes to easily traverse the plasma membrane under the pretense of

being a self-protein. In this study they mixed SWCNTs and the cytochrome c protein in order for them to form a complex. Cytochrome c is normally released from the mitochondria when a cell intends to undergo apoptosis. The cells succumbed to apoptosis once cytochrome c was endocytosed and released from the endosome into the cytoplasm (Kam & Dai, 2005). CNTs have many drug-delivery applications; therefore, specificity in cell recognition, endosomal release and degradation are equally important to ensure high efficiency of these drugs and to safeguard against toxicity. Cell culture experiments were further done to investigate the effect of topical applications of short and long CNTs on the human airway epithelial and colon carcinoma cell lines (Kam & Dai, 2005).

The Calu-3 cell line was characterized before conducting the CNT dose response in order to assess its physiological similarity to the original tissue. Stimulation of Calu-3 cells with epinephrine activates the cAMP/PKA dependant chloride secretion pathway (Shen et al., 1994). Therefore, increases in cAMP in this cell-line served to confirm that the end stage activation of CFTR was via this pathway, Fig 19. Epinephrine binds to its basolateral surface receptor. Then a first messenger G protein binds to its receptor on the catalytic domains of adenylyl cyclase and in turn activates adenylyl cyclase. AC catalyzes the transformation of ATP cAMP, a second messenger. cAMP is released into the cytoplasm and binds PKA to expose this enzyme's active site (Sadava et al., 2009). PKA goes on to phosphorylate CFTR, which allows the movement of Cl^- ions to the apical surface (Gadsby & Nairn, 1999). Forskolin also increases chloride secretion via the cAMP/PKA pathway. Other cAMP- independent effects of forskolin include inhibition of glucose transport and modulation of ligand and voltage-gated ion channels (Laurenza, Sutkowski & Seamon, 1989). The diversity of the effect of forskolin makes it an

important reagent; however, epinephrine also has more than one function, serving as a neurotransmitter and a hormone. Epinephrine was found to be just as potent as forskolin in causing an increase in the cell's total stimulated SCC, Figs. 7 and 8. However, the native hormone was used as the stimulant to conduct further hormonal and CNTs dose dependent studies.

Pretreatment with amiloride did not result in any changes in baseline or stimulated SCC, this indicates that there is no sodium absorption in that cell line, Fig. 9.

U73122 is the inhibitor for phospholipase C (PLC). PLC is a calcium-regulating enzyme. It hydrolyzes phosphatidylinositol 4,5-biphosphate (PIP_2) into two second messengers, inositol 1,4,5-trisphophate (IP_3) and diacylglycerol (DAG). IP_3, in turn, activates the release of calcium from intracellular stores (Fukami, Inanobe, Kanemaru, & Nakamura, 2010). Therefore, pretreatment of the Calu-3 cells with the inhibitor caused depletions in intracellular calcium. When the Calu-3 cells were further stimulated with epinephrine there was a large difference in the first peak in the inhibitor treated cells, compared to the control. When the U73122 was added along CFTR inh-172, the total first peak was nearly wiped out. This indicated that the first peak was mainly due to the two chloride channels, CFTR and CaCCs, Fig. 10a.

Pretreatment with ionomycin caused increases in the chloride secretion oscillations, except the first peak. Ionomycin is an ionophore which increases intracellular calcium levels. Calu-3 cells were treated with this reagent then stimulated with epinephrine. The resultant first peak was less prominent than the second and indicated that this first peak was not entirely influenced by CaCCs, Fig. 12. When Bapta-AM, a calcium chelator, was preincubated with the cells, all the peaks were decreased,

indicating that they were all influenced by the CaCC action, Fig. 13. These data indicate

that secretions from both CaCC and CFTR contribute to the total chloride secretion.

Many studies have shown that CFTR and CaCC are interacting and that CFTR controls

CaCC by attenuating its action (Kunzelmann et al., 1997; Wei et al., 1999; Wei et al.,

2001). Preincubation with both CFTR inh-172 and tannic acid caused a decrease in the

total SCC, showing that the two channels are controlling the cell line's total current, Figs.

14 to 16.

Further studies were done to investigate the total apical fluid secretion which

resulted due to the movement of Cl^- ions out of the cell. Ion movement is followed by the

movement of water ions and therefore gives rise to the total fluid secretion. The data

showed that the control volume was not significantly larger than the experimental

volumes, Figs. 17 and 18. The total fluid secretion was expected to be larger in the 2 min

and 5 min stimulated samples. The similarity in fluid volumes between the control and

experimental samples may be due to the dynamic chloride secretion that occurs in un-

stimulated Calu-3 cells. Lung fluid is secreted into the lung by the net movement of Cl^-

ions and establishes an osmotic gradient (Liu *et al*., 2003)

Confluent Calu-3 cells which were incubated with the nanotubes for 48 h showed

marked changes in the measured TEER and stimulated SCC. Calu-3 cells typically have

resistances between 500 and 800 $\Omega.cm^2$, and when maintained at an air-liquid interface

they produce well developed tight junctions between cells. After 48 h of incubation, the

SWCNTs caused a decrease in TEER at concentrations ranging from 4 $\mu g/cm^2$ – 0.04

ng/cm^2. 24 hr incubations caused a similar decrease except that there was no effect seen

for the 0.4 $\mu g/cm^2$ and 0.4 ng/cm^2 concentrations. The MWCNTs caused significant

decreases in TEER in the 4 µg/cm^2 – 0.04 ng/cm^2 range for the 48 h incubation time point

and 0.04 µg/cm^2 – 0.4 ng/cm^2 for the 24 h time point. These changes in TEER indicate

that the barrier function of the cell monolayer had been impaired by the CNTs. The

epithelial barrier is our first line of defense against invading microorganisms or materials;

hence, if there is a breakdown in this line of defense, there will be damage of or an

invasion into the underlying tissue or system. The agglomerating nature of the nanotubes

may make it difficult to get rid of them. Blazer-Yost et al. (2011) explained that at

concentrations above 0.4µg/cm^2 nanotubes formed large clumps that were visible without

microscopes while at lower concentrations they were dispersed.

While there were significant decreases in stimulated SCC in the Calu-3 cell line,

due to CNTs exposures, the chloride channels still remained functional. Figs. 20 to 22

show that the baseline SCC current was unaffected by CNT exposures. This baseline

current is due to the dynamic ion flux across the cells. The stimulated SCC was

significantly decreased by the CNT exposures. This stimulated SCC was under Cl$^-$

channel control, indicating that the chloride may have been affected. Amos et al. (2008)

showed that when the MPK cells were exposed to extremely high concentrations of NPs

(200µg/cm^2), their proteomic changes in proteins were related to junctional and cell

adhesion functions (as cited in Blazer-Yost et al., 2011, p. 13). These affected proteins

are cell membrane or intracellular proteins. It can be derived that CNTs may be affecting

the cell by disrupting the membrane proteins. Decreased TEER values also indicate that

the CNTs may be disrupting the tightness of the junctional complexes, and therefore the

physical structure and the hormonal function of the cells. These data suggest that the

CNTs have the potential to disrupt the chemical and physical integrity of the epithelial

tissue. Rotoli et al., (2008) previously showed that MWCNTs decreased paracellular permeability in Calu-3 cells. In their study, they showed that these CNTs did not affect Calu-3 cell viability compared to its effect on two comparable cell lines, THP-1 human macrophages (THP -1) and human endothelial cells from umbilical vein (HUVECs). These cells were cultured for 24 h and the Calu-3 cells were cultured for 48 h. All cell lines were exposed to 100 μg/ml of carbon black, SWCNTs or MWCNTs. Significant changes were noted for only the THP -1 and HUVECs cell lines.

Dose response experiments were done on another epithelial cell line, the T84 cell line. This cell line has been widely used as a model for transepithelial anion transport. Confluent T84 cells generally exhibit resistances between 400 and 1200 $\Omega.cm^2$ (Madara & Stafford, 1989). Their SCC is wholly representative of the chloride secretion in their apical membrane (Barrett, 1993; Dharmsathaphorn, McRoberts, Mandel, Tisdale, & Masui, 1984).

T84 cells were stimulated with secretin in order to measure its hormonal responsiveness to the stimulant. Secretin binds to its basolateral surface receptor and causes the activation of CFTR via the cAMP/PKA pathway (Shen et al., 1994). Further pretreatment was done with amiloride, which resulted in a small decrease in the baseline SCC, indicating that there was sodium absorption contributing to the baseline SCC. However, after stimulating the cells with secretin, there was no significant difference in stimulated SCC in the experimental group compared to that of the control, Fig. 24. T84 cells are derived from a human colon carcinoma (Dharmsathaphorn et al., 1984). A study conducted by Kunzelmann, Kathöfer, Hipper, Gruenert, and Greger (1996) demonstrated that T84 cells grown in primary cultures showed decreased amiloride sensitivity over

time. They explained that it is possible that T84 cells may have lost their sodium absorption capacity after several passages of cell culturing, or because of the fact that they were derived from tumor cells.

To measure the sensitivity of the active channels in the T84 cell line, cells were pretreated with a non-specific chloride channel inhibitor, NPPB. After a 10 min pretreatment with NPPB, the cells were stimulated with secretin. The stimulation resulted in a further decline in SCC after a very small peak. The data showed that the stimulated SCC was due to chloride secretion, Fig. 25. Further assessment done to determine the identity of the chloride channels showed that after pretreatment with the CFTR inhibitor, GlyH-101, there was a decrease in the baseline and stimulated SCC. This chloride channel inhibitor, however, failed to completely inhibit the total stimulated SCC, Fig. 27. Treatment with the TMEM16-a inhibitor, tannic acid, showed that there was no difference in the baseline and the stimulated SCC peak compared to that of the control, Fig. 26. Therefore, a more specific inhibitor for the CFTR channel was used. Pretreatment with CFTR inh-172 alone and CFTR inh-172 along with tannic acid showed a greater inhibition of the chloride channels. This showed that theT84 cell line's stimulated SCC is predominantly due to chloride secretion via CFTR, Fig. 28 and 29. Therefore, the dominant channel in this cell line is CFTR. CFTR is the main channel contributing to the stimulated SCC in the T84 cell line. After identifying the channels that are involved in the T84 cell line, the effect of CNTs on the cell line was measured.

Short raw, pristine or acid treated multi-wall CNTs were incubated with the cells for 48 h prior to electrophysiology measurements. There were no significant changes in the baseline or stimulated SCC of treated cells compared with control. TEER remained

unaffected as well. The high resistivity of the cell line may be due to the fact that colon cells have high resistances and also contain a mucus covering. Krug and Wick (2009) explained that ingestion is a less significant portal of entry for NPs compared to inhalation; however, the majority of the NPs which are cleared from the lungs by the mucociliary clearance mechanism enter the gastrointestinal tract (GI) when the individual swallows mucus filled with lung debris. The thick mucus may prevent the nanotubes from interacting with the epithelial lining. While this mucus may be broken down in the stomach, the intestinal GI track epithelium also contains a mucus covering (glycoproteins) which serves to protect it from proteases and gastric acid. This layer may also function to protect the colon from NPs. T84 cells exhibit a thick mucus layer when they become confluent; therefore, this may contribute to their high resistance to the CNTs doses. Jachak et al. (2012) showed that nanoparticles are trapped in the mucus lying on top of human epithelial cells. In that study, the diffusion coefficients of three different metal oxides (nMeOs) and two types of SWCNTs was measured in undiluted human mucus. The results showed that while zinc oxide moved fast enough to penetrate the mucus layer, the mucus efficiently trapped the CNTs. These data supports my findings to show that the thick enteric mucus layer may be trapping the invading CNTs.

The cytokine assays also confirmed that the CNTs had no toxic effects on this cell line. The cells showed no significant levels of IL-8 and TNF-α leakage after 48 h exposures. Since CNTs entered the body via the lungs more often, their effects on the Calu-3 cell line was used as a platform for investigating their effect on the cell membrane by using model membranes.

Biophysical measurements were done to elucidate the potential interaction between CNTs and the plasma membrane. The membrane is the cellular barrier against foreign materials. Therefore, measurements were conducted to understand how the CNTs may be interacting with the cell by investigating the CNT- membrane interaction by using model lipid membranes. The model membranes were formed in a hole in the Teflon tape in a two well BLM chamber made of Teflon blocks. The wells were separated by the Teflon tape, which has a thickness within the range of 0.02 to 0.12mm, and the holes had diameters ranging from 0.04 to1.2 mm. KCl buffer was added to each well and lowered below the hole in the Teflon tape. The lipid, dissolved in pentane, was added to each well in the chamber. Pentane is a volatile organic solvent, and it was allowed to evaporate. After five min, the lipids that were left formed a monolayer on the surface of the buffer, orienting their head groups- the hydrophilic end, to face the solvent, and their tail groups- the hydrophobic end, were held away from the solvent's surface. Bilayer lipid membranes were formed as the solvent on either side of the Teflon partition was raised above the hole. The lipids became lodged within the hole in the tape, allowing the hydrocarbon chains to oppose the aqueous phase; hence, a lipid bilayer, being the most favorable conformation, was formed. Raising the solvent above the opening serves to maintain this electrically favorable bilayer arrangement within the opening.

In order to measure the electrical currents across the membrane, two electrodes were placed in each well and applied a recurring voltage pulse to the membrane, and the resultant current was noted from the storage oscilloscope (Montal, & Mueller, 1972). The first 62s of the graph in Fig. 37 shows the resultant flat base line of a stable membrane that was generated by pCLAMP 10 Electrophysiology Data Acquisition and

Analysis Software. The increases and decreases in currents generated by GA during time = 62s to 68s are caused by the insertions of GA monomers into the membrane. GA is formed from two monomers that bind to each other, across the lipid bilayer, to form a dimer. The dimer generally measures ~2.2 nm, which is a little over half of the thickness of a membrane, approximately 4nm. This protein is a member of the linear GA family. These antibiotics target bacterial plasma membrane and increase cation permeability by forming bilayer spanning channels. This protein serves as an ideal atomic-level model for channel structure due to the single-stranded beta-helical dimer it forms, which allows them to be studied as bilayer spanning channels (Andersen, 1984). The formation of a GA channel is hence dependent on thickness of the membrane and overall the bilayer environment. The GA monomers have to reach each other across the membrane in order to form the channel. If a multilayered membrane forms, this will increase the difficulty of the monomers to form dimers. The formation of multilayered membranes was noted when the capacitance reading of a BLM instantly doubled. This was generally followed by a decrease in GA channel formations, and at this point the membranes had to be rebuilt.

The interaction of the CNTs with the membrane caused electrical deflections. Figs. 38 and 39 show that there were large electrical deflections in the CNT treated membranes. The nanotubes were added to each well on either side of the membrane and then stirred for 5 to 10 seconds, using a small magnetic stir bar. This allowed even distribution of the CNTs in the wells. While it was clear that there were interruptions in the membrane, it was not clear how the CNT-membrane interactions occurred. The deflections in the membranes were very random and occurred for various lengths of time.

It was also noted that the amount of current that was allowed to cross the membrane in the presence of the CNTs varied. However, a single open GA channel allowed approximately 2pA to cross the membrane at a time. When the simultaneous opening of multiple GA channels was observed, the total current closely doubled the number of channels that were seen on the trace.

One study illustrated that water ion transport was possible through the hydrophobic channels of modified carbon nanotubes. There was an asymmetrical placement of charges on the nanotubes which was inspired by the charge distribution of aquaporin. This charge distribution served to allow the free flow of water independent of the water molecules' orientations. Zuo, Shen, Ma and Guo (2009) explained that aquaporins regulate the osmotic gradients across cell membranes by passive transport but are not able to serve as pumps or transport water unidirectionally. These findings show that the CNTs may serve as channels for unregulated water movement across the membrane. While aquaporins are able to restore homeostatic imbalances by regulated water movement in the membrane, CNTs are only able to move water in one direction due to the influence of charge distributions.

In a separate study it was explained that ion movements through channels are regulated by surrounding proteins; for instance, the transport of K^+ is stabilized by polar interactions with surrounding proteins, a feature that is generally absent in unfunctionalized nanotubes (Joseph, Mashl, Jakobsson, & Aluru, 2003). Overall, while the nanotubes have the potential to serve as ion channels, they rendered unregulated, random ion movement across the BLM, as was illustrated in Figs. 38 and 39.This movement may also be influenced by charge distribution along the nanotube.

Wang, Zhang, Bae and Granick (2008) illustrated that the surface charge on the interacting CNTs could alter the phase of the lipids and therefore the overall membrane function. Amine modified (positively charged; ~ 0.25 e^+/nm^2) and carboxyl modified (negatively charged; 0.91 e^-/nm^2) polystyrene NPs were added to a phospholipid bilayer made with the neutral lipid DOPC (dioleoyl PC). The cationic NPs caused a reduction in lipid density while the anionic NPs increased lipid density. In a separate previous study Debouzy, Crouzier and Flahaut (2009) showed that CNTs also had the potential to alter the fluidity of the lipid composition in membranes. An ^{2}H NMR (nuclear resonance screening) spectra of the lipid dimyristoyl phosphatidyl Choline (DMPC) illustrated a typical phospholipid bilayer below phase transition (196 K), in comparison with a spectra recorded in similar condition with CNTs present. The second spectra showed decreased values of resonance, resulting in an overall 2 Kelvin decrease in the transition phase temperature. This temperature change indicated an overall increase in fluidity of the lipid bilayer.

In Table 1 and 2 the Zeta potential values reported for all NPs showed that the nanotubes all had a surface charge of approximately -8mV. This value suggests that the CNTs may affect lipid density of the bilayer. The changes in the membrane lipid density could further affect membrane proteins.

 The fragments observed in the TEM images were shorter than 100nm and this showed that there was an increased potential for them to serve as membrane channels because of their smaller sizes. This would increase their chances to completely cross the membrane and in doing so allow the escape of ions across the insulated bilayer. The TEM images in Figs. 4 and 6 show that the protein coats the nanotubes. The NP-proteins'

coronas allows them to be more susceptible to crossing a plasma membrane because of improved biocompatibility (Kam & Dai, 2005; Ge, 2011). This coating may increase the membrane spanning potential of the NPs and, therefore, they may serve as transient channels in the model membrane.

Plasma membranes are made up of various ratios of lipid-protein combinations, depending on the origin of the tissue. Measurements were done to investigate the possible effect of CNTs on membrane proteins by using the ion channel reporter protein GA. In a previous study GA was used to compare the differences in conductance of the negatively charged lipid, DPhPS, and the uncharged lipid, DPhPC. The research findings showed that at low electrolyte concentrations the channel conductance is greater in the charged membrane than in the neutral membrane. The surface charge tends to influence the accumulation of counter ions, whereas ions of the same sign are depleted. The enhancement of the conductance is much larger when negatively charged lipids surround a neutral channel; hence, the transport rate of the counter ions through the GA channel is greatly enhanced (Apell, Bamberg & Läuger, 1979).

In Figs. 42 and 43 it is noted that the GA behaves differently in PC and PS lipids, with different channel numbers and open probabilities. DPhPC was more stable and allowed more single channels and smaller multiples of channels to be formed at a given time, whereas DPhPS had lower numbers of single channels and larger numbers of multiple channels open in the membrane at a single time. The probability values reported in Table 4 show the open or closed conformation of the channels at a given time. The reported probabilities were all within the range of 0 to 0.5; hence, they were all predominantly closed. These data show that the channels had a short lifetime in the

membrane. The data also showed that the average maximum channel number for DPhPC, 82.5, was less that that reported for the DPhPS lipid, which was 105 channels. These values align with the data described by Apell et al., (1979). Their study illustrated that neutral lipids allowed more stable channel formations, whereas negatively charged lipids greatly influenced the changes in the channel formation. Here these data show that lipid charge influences the channel conductance as well as channel number. Further analysis was done to investigate the effect of CNTs on GA in the DPhPC BLM.

When the nanotubes were added to the DPhPS lipid, the BLM had been pretreated with GA for at least 0.5 h. In some cases the current increased, and in others there was immediate lysing of the membrane. This finding suggests that there were interactions between the charges on the protein coated nanotubes and the negatively charged membrane lipids. The protein-coated nanotubes may possibly be inundating the membrane and thereby causing large ion fluxes across the bilayer. The interaction of the CNTs with the DPhPC BLM showed instability in the GA channel conductance compared to the pure GA channel conductance. Fig. 45 shows that while the membrane was not immediately broken, the channel open and close probability was severely changed, and finally the membrane broke after 21 min. The data were not compatible with the theoretical graphs that were generated by the binomial distribution formula; hence, the maximum channel number and channel open probability were not able to be determined for many traces.

Fig. 46 shows that while the amplitude of the channels increased, the defined channels were not able to be discerned. An important feature of the graph was that there was a steady increase in the baseline. There were also characteristic spikes which had

been observed in the bare membrane which was exposed to only CNTs (Figs. 38 and 39).

Along with these spikes the membrane channel number continued to steadily increase,

indicating that more current was allowed to move across the membrane.

CHAPTER 5. CONCLUSIONS

Carbon nanotubes have the ability to undergo surface modification when they enter a biological environment by forming protein coronas with the surrounding proteins. The TEM images showed that these protein coronas were formed when long SWCNTs and short MWCNTs were mixed with cell culture media. *In vitro* biologically modified long single-walled and multi-walled CNTs caused marked decreases in stimulated SCC and TEER in human airway epithelial cells. The T84 cells remained unaffected by the short MWCNTs. The short MWCNTs also showed increased ion channel number in the neutral lipid and affected the channel open and close conformations in model lipid membranes. These finding may serve as a platform for understanding the potential toxicity of raw or pristine CNTs which are commonly used in biomedical fields and many other application of the quickly developing nanotechnology industry.

REFERENCES

REFERENCES

Andersen, O. S. (1984). Gramicidin Channels. *Annual Review of Physiology*, *46*(1), 531-548.

Artursson, P., & Karlsson, J. (1991). Correlation Between Oral Drug Absorption in Humans and Apparent Drug Permeability Coefficients in Human Intestinal Epithelial (Caco-2) Cells. *Biochemical and Biophysical Research Communications*, *175*(3), 880-885.

Banga, A., Witzmann, F. A., Petrache, H. I., & Blazer-Yost, B. L. (2012). Functional Effects of Nanoparticle Exposure on Calu-3 Airway Epithelial Cells. *Cellular Physiology and Biochemistry*, *29*(1-2), 197-212.

Barrett, K. E. (1993). Positive and Negative Regulation of Chloride Secretion in T84 Cells. *American Journal of Physiology-Cell Physiology*, *265*(4), C859-C868.

Baughman, R. H., Zakhidov, A. A., & de Heer, W. A. (2002). Carbon Nanotubes-the Route Toward Applications. *Science*, *297*(5582), 787-792.

Bebok, Z., Collawn, J. F., Wakefield, J., Parker, W., Li, Y., Varga, K., Sorscher, E. J., & Clancy, J. P. (2005). Failure of cAMP Agonists to Activate Rescued ΔF508 CFTR In CFBE41o–Airway Epithelial Monolayers. *The Journal of Physiology*, *569*(2), 601-615.

Bhabra, G., Sood, A., Fisher, B., Cartwright, L., Saunders, M., Evans, W. H., Surprenant A., Lopez-Castejon, G., Mann, S., Davis, S. A., Hails, L. A., Ingham, E., Verkade, P., Lane, J., Heesom, K., Newson, R., & Case, C. P. (2009). Nanoparticles Can Cause DNA Damage Across a Cellular Barrier. *Nature Nanotechnology*, *4*(12), 876-883.

Blazer-Yost, B. L., Banga, A., Amos, A., Chernoff, E., Lai, X., Li, C., Mitra S., & Witzmann, F. A. (2011). Effect of Carbon Nanoparticles on Renal Epithelial Cell Structure, Barrier Function, and Protein Expression. *Nanotoxicology*, *5*(3), 354-371.

Chen, J. L., Ahluwalia, J. P., & Stamnes, M. (2002). Selective Effects of Calcium Chelators on Anterograde and Retrograde Protein Transport in the Cell. *Journal of Biological Chemistry*, 277(38), 35682-35687Chen, Y., Iqbal, Z., & Mitra, S. (2007). Microwave-Induced Controlled Purification of Single-Walled Carbon nanotubes without Sidewall Functionalization. *Advanced Functional Materials*, *17*(18), 3946-3951.

Coccini, T., Manzo, L., & Roda, E. (2013). Safety Evaluation of Engineered Nanomaterials for Health Risk Assessment: An Experimental Tiered Testing Approach Using Pristine and Functionalized Carbon Nanotubes. *ISRN Toxicology*, *2013*.

Dalton, A. B., Collins, S., Munoz, E., Razal, J. M., Ebron, V. H., Ferraris, J. P., Coleman J. N., Kim B. G., & Baughman, R. H. (2003). Super-Tough Carbon-Nanotube Fibres. *Nature*, *423*(6941), 703-703.

Davis, J. J., Green, M. L., Allen O Hill, H., Leung, Y. C., Sadler, P. J., Sloan, J., Xavier A. V., & Chi Tsang, S. (1998). The Immobilisation of Proteins in Carbon Nanotubes. *Inorganica Chimica Acta*, *272*(1), 261-266.

Davis, J. M., & McDonald, J. C. (1988). Low Level Exposure to Asbestos: is There a Cancer Risk?. *British Journal of Industrial Medicine*, *45*(8), 505.

Dawson, K. A., Salvati, A., & Lynch, I. (2009). Nanotoxicology: Nanoparticles Reconstruct Lipids. *Nature Nanotechnology*, *4*, 84-85.

Debouzy, J. C., Crouzier, D., & Flahaut, E. (2010). Hydrophobic Double Walled Carbon Nanotubes Interaction with Phopholipidic Model Membranes: ^{1}H-, ^{2}H-, ^{31}P NMR and ESR Study. *Environmental Toxicology and Pharmacology*, *30*(2), 147-152.

Dharmsathaphorn, K. I. E. R. T. I. S. I. N., McRoberts, J. A., Mandel, K. G., Tisdale, L. D., & Masui, H. (1984). A Human Colonic Tumor Cell Line that Maintains Vectorial Electrolyte Transport. *American Journal of Physiology-Gastrointestinal and Liver Physiology*, *246*(2), G204-G208.

Eckmann, L., Kagnoff, M. F., & Fierer, J. (1993). Epithelial Cells Secrete the Chemokine Interleukin-8 in Response to Bacterial Entry. *Infection and Immunity*, *61*(11), 4569-4574.

Egan, M., Flotte, T., Afione, S., Solow, R., Zeitlin, P. L., Carter, B. J., & Guggino, W. B. (1992). Defective Regulation of Outwardly Rectifying Cl− Channels by Protein Kinase A Corrected by Insertion of CFTR. *Nature*, *358*(6387), 581-584.

Fei, L., & Perrett, S. (2009). Effect of Nanoparticles on Protein Folding and Fibrillogenesis. *International Journal of Molecular Sciences*, *10*(2), 646-655.

Fukami, K., Inanobe, S., Kanemaru, K., & Nakamura, Y. (2010). Phospholipase C is a Key Enzyme Regulating Intracellular Calcium and Modulating the Phosphoinositide Balance. *Progress in Lipid Research,* 49(4), 429-437.

Gadsby, D. C., & Nairn, A. C. (1999). Control of CFTR Channel Gating by Phosphorylation and Nucleotide Hydrolysis. *Physiological Reviews*, *79*(1), S77-S107.

Ge, C., Du, J., Zhao, L., Wang, L., Liu, Y., Li, D., Yang Y., Zhou R., Zhou Y., Chai Z., & Chen, C. (2011). Binding of Blood Proteins to Carbon Nanotubes Reduces Cytotoxicity. *Proceedings of the National Academy of Sciences*, *108*(41), 16968-16973.

Geer LY, Marchler-Bauer A, Geer RC, Han L, He J, He S, Liu C, Shi W, Bryant SH. The NCBI BioSystems database. *Nucleic Acids Res.* 2010 Jan; 38(Database issue):D492-6.*(Epub 2009 Oct 23)* [PubMed PMID: 19854944]

Girshman, J., Greathouse, D. V., Koeppe, R. E., & Andersen, O. S. (1997). Gramicidin Channels in Phospholipid Bilayers with Unsaturated Acyl Chains. *Biophysical Journal*, *73*(3), 1310-1319.

Gstraunthaler, G. (2003). Alternatives to the use of Fetal Bovine Serum: Serum-Free Cell Culture. *Altex*, *20*(4), 275-281.

Hall, J. L. & Baker, D. A. (1977). Integrated Themes in Biology: Cell Membranes and Ion Transport . (p 24-28) London: Longman Group Limited.

Harrison L. M., Rallabhandi P., Michalski J., Zhou X, Steyert S. R., Vogel S. N. & Kaper JB.(2008). Vibrio cholerae Flagellins Induce Toll-Like Receptor 5-Mediated Interleukin-8 Production through Mitogen-Activated Protein Kinase and NF-$_k$B Activation. *American Society for Microbiology.* 76 (12), 5524-5534

Hirano, S., Kanno, S., & Furuyama, A. (2008). Multi-Walled Carbon Nanotubes Injure the Plasma Membrane of Macrophages. *Toxicology and Applied Pharmacology*, *232*(2), 244-251.

Iordache, C., & Duszyk, M. (2007). Sodium 4-Phenylbutyrate Upregulates Enac and Sodium Absorption in T84 Cells. *Experimental Cell Research*, *313*(2), 305-311.

Jachak, A., Lai, S. K., Hida, K., Suk, J. S., Markovic, N., Biswal, S., & Hanes, J. (2012). Transport of Metal Oxide Nanoparticles and Single-Walled Carbon Nanotubes in Human Mucus. *Nanotoxicology*, *6*(6), 614-622.

Jaideep, R. (2011). Commercialisation of Nanotechnology: Global Overview and European Position [PDF document]. Retrieved from: http://www.euronanoforum2011.eu/wp-content/uploads/2011/09/enf2011_support-commercialisation_raje_fin.pdf (Accessed April 8, 2013)

Joseph, S., Mashl, R. J., Jakobsson, E., & Aluru, N. R. (2003). Electrolytic Transport in Modified Carbon Nanotubes. *Nano Letters*, *3*(10), 1399-1403.

Kam, N. W. S., & Dai, H. (2005). Carbon Nanotubes as Intracellular Protein Transporters: Generality and Biological Functionality. *Journal of the American Chemical Society*, *127*(16), 6021-6026.

King, L. S., & Yasui, M. (2002). Aquaporins and Disease: Lessons from Mice to Humans. *Trends in Endocrinology & Metabolism*, *13*(8), 355-360.

Klaus, G. G., O'Garra, A., Bijsterbosch, M. K., & Holman, M. (2005). Activation and Proliferation Signals in Mouse B Cells VIII. Induction of DNA Synthesis in B Cells by a Combination of Calcium Ionophores and Phorbol Myristate Acetate. *European Journal of Immunology*, *16*(1), 92-97.

Komalavilas, P., Mehta, S., Wingard, C. J., Dransfield, D. T., Bhalla, J., Woodrum, J. E., Molinaro J. R., & Brophy, C. M. (2001). PI3-Kinase/Akt Modulates Vascular Smooth Muscle Tone via cAMP Signaling Pathways. *Journal of Applied Physiology*, *91*(4), 1819-1827.

Kosynkin, D. V., Higginbotham, A. L., Sinitskii, A., Lomeda, J. R., Dimiev, A., Price, B. K., & Tour, J. M. (2009). Longitudinal Unzipping of Carbon Nanotubes to Form Graphene Nanoribbons. *Nature*, *458*(7240), 872-876.

Krug, H. F., & Wick, P. (2011). Nanotoxicology: An Interdisciplinary Challenge. *Angewandte Chemie International Edition*, *50*(6), 1260-1278.

Kunzelmann, K., Kathöfer, S., Hipper, A., Gruenert, D. C., & Greger, R. (1996). Culture-Dependent Expression of Na+ Conductances in Airway Epithelial Cells. *Pflügers Archiv*, *431*(4), 578-586.

Kunzelmann, K., Mall, M., Briel, M., Hipper, A., Nitschke, R., Ricken, S., & Greger, R. (1997). The Cystic Fibrosis Transmembrane Conductance Regulator Attenuates the Endogenous Ca^{2+} Activated Cl^- Conductance of Xenopus Oocytes. *Pflügers Archiv European Journal of Physiology*, *435*(1), 178-181.

Langecker, M., Arnaut, V., Martin, T. G., List, J., Renner, S., Mayer, M., Dietz, H., & Simmel, F. C. (2012). Synthetic Lipid Membrane Channels Formed by Designed DNA Nanostructures. *Science*, *338*(6109), 932-936.

Laurenza, A., Sutkowski, E. M., & Seamon, K. B. (1989). Forskolin: A Specific Stimulator of Adenylyl Cyclase or a Diterpene with Multiple Sites of Action?. *Trends in Pharmacological Sciences*, *10*(11), 442.

Li, H., Sheppard, D. N., & Hug, M. J. (2004). Transepithelial Electrical Measurements with the Ussing Chamber. *Journal of Cystic Fibrosis*, *3*, 123-126.

Liang, W., Bockrath, M., Bozovic, D., Hafner, J. H., Tinkham, M., & Park, H. (2001). Fabry-Perot Interference in a Nanotube Electron Waveguide. *Nature*, *411*(6838), 665-669.

Liedtke, C. M., & Cole, T. S. (1998). Antisense Oligonucleotide to PKC-E Alters cAMP-Dependent Stimulation of CFTR in Calu-3 Cells. *American Journal of Physiology-Cell Physiology*, 275(5), C1357-C1364.

Liu, H., Hooper, S. B., Armugam, A., Dawson, N., Ferraro, T., Jeyaseelan, K., Thiel A., Koukoulas, I., & Wintour, E. M. (2004). Aquaporin Gene Expression and Regulation in the Ovine Fetal Lung. *The Journal of Physiology*, *551*(2), 503-514.

Liu, J., Rinzler, A. G., Dai, H., Hafner, J. H., Bradley, R. K., Boul, P. J., Lu, A., Iverson, T., Shelimov, K., Huffman, C. B., Rodriguez-Macias, F. Shon, Y., Lee, T. R, Colbert, D. T. & Smalley, R. E. (1998). Fullerene Pipes. *Science*, *280*(5367), 1253-1256.

Liu, W., Rose, J., Plantevin, S., Auffan, M., Bottero, J. Y., & Vidaud, C. (2013). Protein Corona Formation for Nanomaterials and Proteins of a Similar size: Hard or Soft Corona?. *Nanoscale*, *5*(4), 1658-1668.

Liu, Z., Tabakman, S., Welsher, K., & Dai, H. (2009). Carbon Nanotubes in Biology and Medicine: In Vitro and in Vivo Detection, Imaging and Drug Delivery. *Nano Research*, *2*(2), 85-120.

Lynch, I., Cedervall, T., Lundqvist, M., Cabaleiro-Lago, C., Linse, S., & Dawson, K. A. (2007). The Nanoparticle–Protein Complex as a Biological Entity; A Complex Fluids and Surface Science Challenge for the 21st Century. *Advances in Colloid and Interface Science*, *134*, 167-174.

Ma, T., Thiagarajah, J. R., Yang, H., Sonawane, N. D., Folli, C., Galietta, L. J., & Verkman, A. S. (2002). Thiazolidinone CFTR Inhibitor Identified by High-Throughput Screening Blocks Cholera Toxin-Induced Intestinal Fluid Secretion. *Journal of Clinical Investigation*, *110*(11), 1651-1658.

Madara, J. L., & Stafford, J. (1989). Interferon-Gamma Directly Affects Barrier Function of Cultured Intestinal Epithelial Monolayers. *Journal of Clinical Investigation*, *83*(2), 724.

Malvern Instruments Ltd., Zetasizer Nano series User Manual (MAN 0317), Issue 2.1, (2004).

Meinkoth, J. L., Alberts, A. S., Went, W., Fantozzi, D., Taylor, S. S., Hagiwara, M., Montminy, M., & Feramisco, J. R. (1993). Signal Transduction through the cAMP-Dependent Protein Kinase. *Molecular and Cellular Biochemistry*, *127*(1), 179-186.

Mogami, H., Mills, C. L., & Gallacher, D. V. (1997). Phospholipase C Inhibitor, U73122, Releases Intracellular Ca2+, Potentiates Ins (1, 4, 5) P3-Mediated Ca2+ Release and Directly Activates Ion Channels in Mouse Pancreatic Acinar Cells. *Biochemical Journal*, 324(Pt 2), 645.

Montal, M., & Mueller, P. (1972). Formation of Bimolecular Membranes from Lipid Monolayers and a Study of their Electrical Properties. *Proceedings of the National Academy of Sciences*, *69*(12), 3561-3566.

Murakami, H., & Masui, H. (1980). Hormonal Control of Human Colon Carcinoma Cell Growth in Serum-free Medium. *Proceedings of the National Academy of Sciences*, *77*(6), 3464-3468.

Namkung, W., Thiagarajah, J. R., Phuan, P. W., & Verkman, A. S. (2010). Inhibition of Ca^{2+}-Activated Cl^- Channels by Gallotannins as a Possible Molecular Basis for Health Benefits of Red Wine and Green Tea. *The FASEB Journal*, 24(11), 4178-4186.

Oiki, S., Koeppe, R. E., & Andersen, O. S. (1995). Voltage-Dependent Gating of an Asymmetric Gramicidin Channel. *Proceedings of the National Academy of Sciences*, *92*(6), 2121-2125.

Panyala, N. R., Peña-Méndez, E. M., & Havel, J. (2008). Silver or Silver Nanoparticles: A Hazardous Threat to the Environment and Human Health. *Journal of Applied Biomedicine*, *6*(3), 117-129.

Paulmichl, M., Li, Y., Wickman, K., Ackerman, M., Peralta, E., & Clapham, D. (1992). New Mammalian Chloride Channel Identified by Expression Cloning. *Nature*, *356*(6366), 238-241.

Păunescu, T. G., Blazer-Yost, B. L., Vlahos, C. J., & Helman, S. I. (2000). LY-294002-Inhibitable PI 3-Kinase and Regulation of Baseline Rates of Na^+ Transport in A6 Epithelia. *American Journal of Physiology-Cell Physiology*, *279*(1), C236-C247.

Poland, C. A., Duffin, R., Kinloch, I., Maynard, A., Wallace, W. A., Seaton, A., Stone V., Brown S., MacNee W., & Donaldson, K. (2008). Carbon Nanotubes Introduced into the Abdominal Cavity of Mice Show Asbestos-Like Pathogenicity in a Pilot Study. *Nature Nanotechnology*, *3*(7), 423-428.

Popov, A. P., Priezzhev, A. V., Lademann, J., & Myllylä, R. (2005). TiO_2 Nanoparticles as an Effective UV-B Radiation Skin-Protective Compound in Sunscreens. *Journal of Physics D: Applied Physics*, *38*(15), 2564.

Qu, G., Bai, Y., Zhang, Y., Jia, Q., Zhang, W., & Yan, B. (2009). The Effect of Multi-walled Carbon Nanotube Agglomeration on their Accumulation in and Damage to Organs in Mice. *Carbon*, *47*(8), 2060-2069.

Rostovtseva, T. K., Petrache, H. I., Kazemi, N., Hassanzadeh, E., & Bezrukov, S. M. (2008). Interfacial Polar Interactions affect Gramicidin Channel Kinetics. *Biophysical Journal*, *94*(4), L23-L25.

Rotoli, B. M., Bussolati, O., Bianchi, M. G., Barilli, A., Balasubramanian, C., Bellucci, S., & Bergamaschi, E. (2008). Non-functionalized Multi-Walled Carbon Nanotubes Alter the Paracellular Permeability of Human Airway Epithelial Cells. *Toxicolgy Letters*, 178(2), 95-102.

Sadava, D., Hillis, D. M., Heller, H. C., & Berenbaum, M. (2009). *Life: The Science of Biology* (pp. 136-139). WH Freeman.

Sargent Jr, J. F. (2011). *National Nanotechnology Initiative (NNI): Overview, Reauthorization, and Appropriations Issues*. DIANE Publishing.

Service, R (2008). Can High-Speed Tests Sort Out Which Nanomaterials are Safe? *Nanotechnology*, 321, 1036-1037.

Shen, B. Q., Finkbeiner, W. E., Wine, J. J., Mrsny, R. J., & Widdicombe, J. H. (1994). Calu-3: A Human Airway Epithelial Cell Line that Shows cAMP-Dependent Cl^- Secretion. *American Journal of Physiology-Lung Cellular and Molecular Physiology*, *266*(5), L493-L501.

Snyder, P. M., Olson, D. R., Kabra, R., Zhou, R., & Steines, J. C. (2004). cAMP and Serum and Glucocorticoid-Inducible Kinase (SGK) Regulate the Epithelial Na^+ Channel Through Convergent Phosphorylation of Nedd4-2. *Journal of Biological Chemistry*, *279*(44), 45753-45758.

Sprague, R. S., Ellsworth, M. L., Stephenson, A. H., & Lonigro, A. J. (2001). Participation of cAMP in a Signal-Transduction Pathway Relating Erythrocyte Deformation to ATP Release. *American Journal of Physiology-Cell Physiology*, *281*(4), C1158-C1164.

Szymczyk, A., Fievet, P., Mullet, M., Reggiani, J. C., & Pagetti, J. (1998). Comparison of two Electrokinetic Methods–Electroosmosis and Streaming Potential–to Determine the Zeta-Potential of Plane Ceramic Membranes. *Journal of Membrane Science*, *143*(1), 189-195.

Taddei, A., Folli, C., Zegarra-Moran, O., Fanen, P., Verkman, A. S., & Galietta, L. J. (2004). Altered Channel Gating Mechanism for CFTR Inhibition by a High-Affinity Thiazolidinone Blocker. *FEBS Letters*, *558*(1), 52-56.

Tantra, R., & Cumpson, P. (2007). The Detection of Airborne Carbon Nanotubes in Relation to Toxicology and Workplace Safety. *Nanotoxicology*, *1*(4), 251-265.

The UniProt Consortium. Reorganizing the protein space at the Universal Protein Resource (UniProt), *Nucleic Acids Res.* 40: D71-D75 (2012).

Ussing, H. H., & Zerahn, K. (1951). Active Transport of Sodium as the Source of Electric Current in the Short-circuited Isolated Frog Skin. *Acta Physiologica Scandinavica*, *23*(2-3), 110-127.

Verma, S. K., Prabhat, K. C., Goyal, L., Rani, M., & Jain, A. (2010). A Critical Review of the Implication of Nanotechnology in Modern Dental Practice. *National Journal of Maxillofacial Surgery*, *1*(1), 41.

Wallace, B. A. (1986). Structure of Gramicidin A. *Biophysical Journal*, *49*(1), 295-306.

Wei, L., Vankeerberghen, A., Cuppens, H., Cassiman, J. J., Droogmans, G., & Nilius, B. (2001). The C-Terminal Part of the R-Domain, but not the PDZ Binding Motif, of CFTR is involved in Interaction with Ca $^{2+}$-Activated Cl^{-} Channels. *Pflügers Archiv European Journal of Physiology*, *442*(2), 280-285.

Wei, L., Vankeerberghen, A., Cuppens, H., Eggermont, J., Cassiman, J. J., Droogmans, G., & Nilius, B. (1999). Interaction between Calcium-Activated Chloride Channels and the Cystic Fibrosis Transmembrane Conductance Regulator. *Pflügers Archiv European Journal of Physiology*, *438*(5), 635-641.

Winterhalter, M. (2000). Black Lipid Membranes. *Current Opinion in Colloid & Interface Science*, *5*(3), 250-255.

Yao, Z., Kane, C. L., & Dekker, C. (2000). High-field Electrical Transport in Single-Wall Carbon Nanotubes. *Physical Review Letters*, *84*(13), 2941-2944.

Zuo, G., Shen, R., Ma, S., & Guo, W. (2009). Transport Properties of Single-File Water Molecules inside a Carbon Nanotube Biomimicking Water Channel. *ACS Nano*, *4*(1), 205-210.